(a) Lisianthus cultivars with a wide range of flower colors used in our study

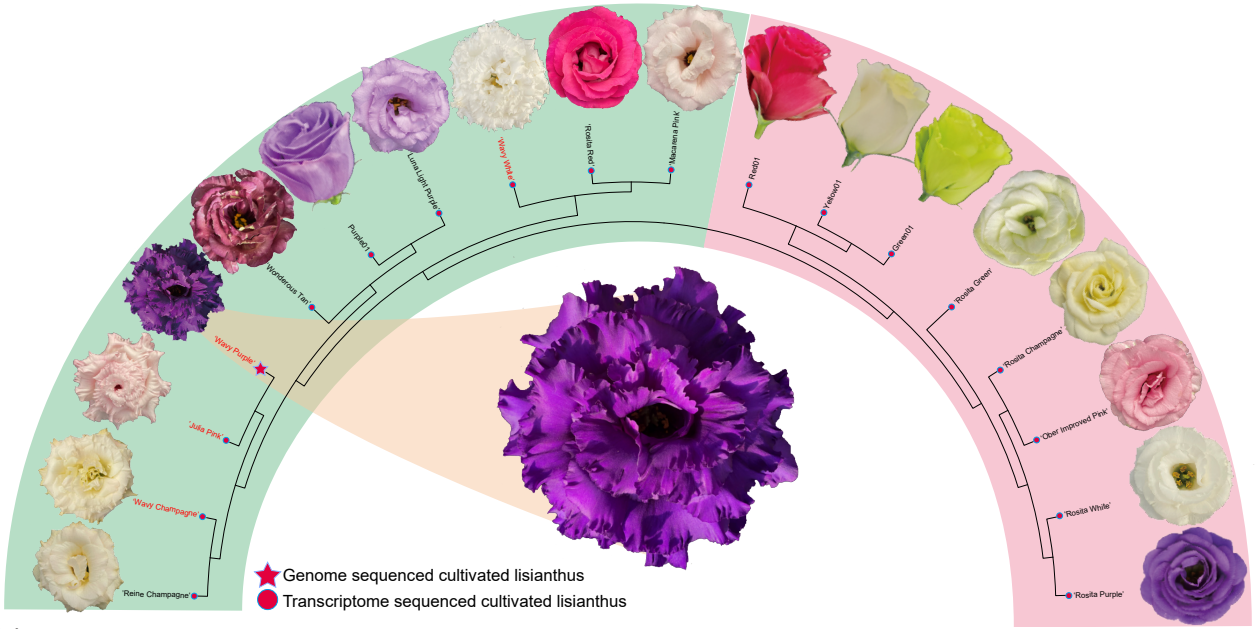

(b)

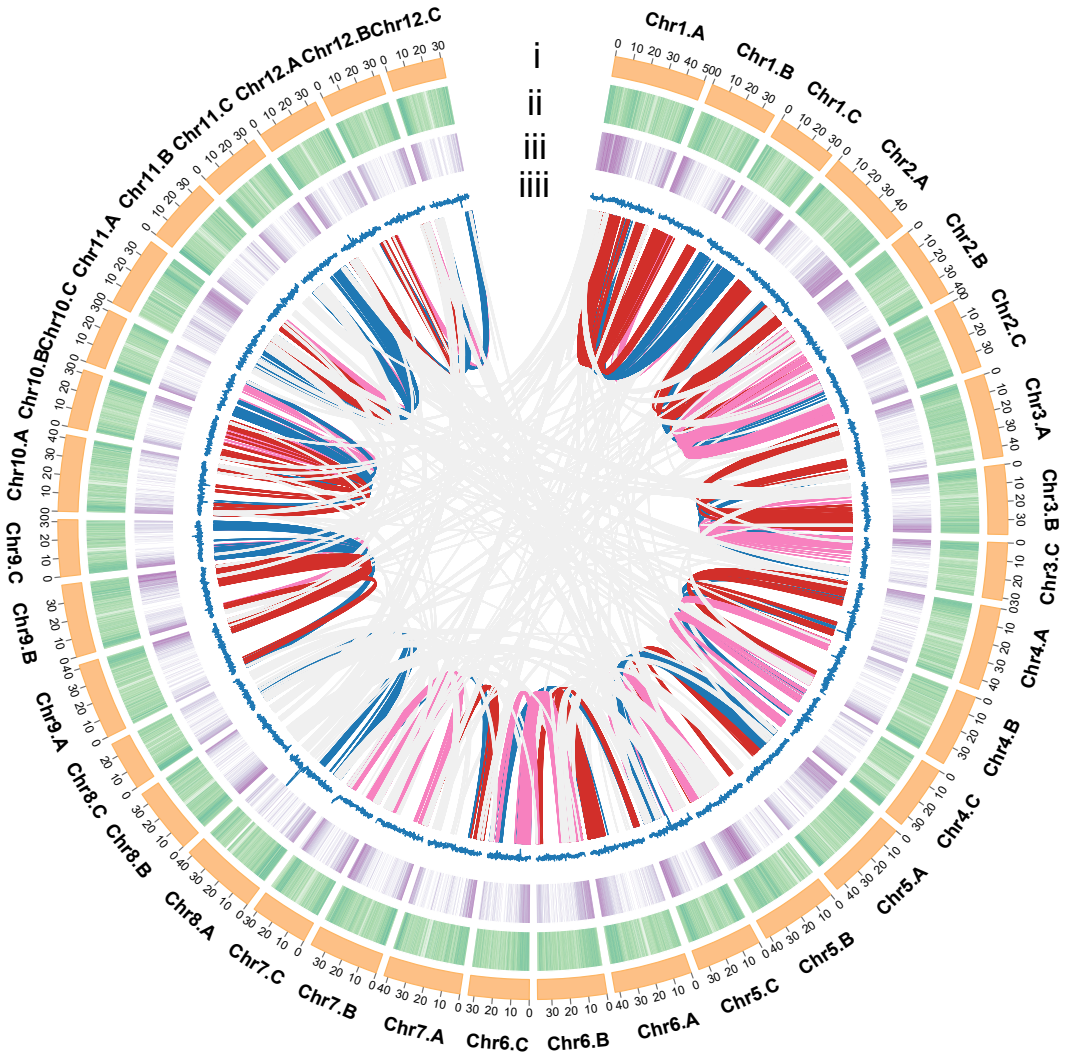

Figure S1. (a) Lisianthus used in our study. Neighbor-joining phylogeny is constructed based on biallelic SNPs of the nuclear genome using transcriptome data. Lisianthus with wave-shaped petals are in red fonts. (b) Genomic characteristics of the *Eustoma grandiflorum* genome along 36 pseudochromosomes. i: chromosomes, ii: gene density, iii: repetitive sequence density, iiii: GC content. Links connect the synteny blocks in the core. Red, blue, and pink ribbons represent synteny blocks between ChrX.A and ChrX.B, ChrX.A and ChrX.C, and ChrX.B and ChrX.C.

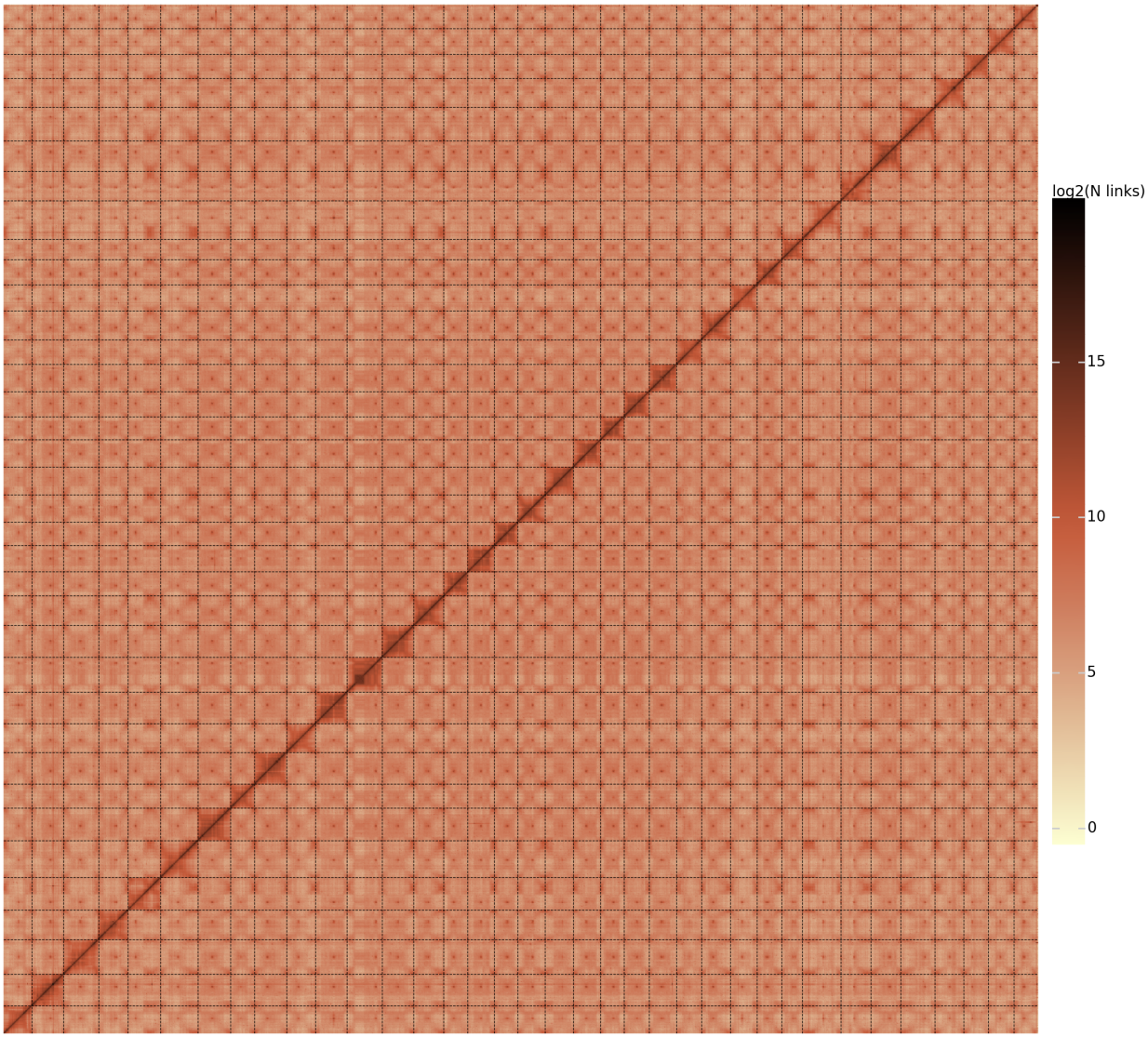

Figure S2. Hi-C interaction heatmap of the *Eustoma grandiflorum* genome.

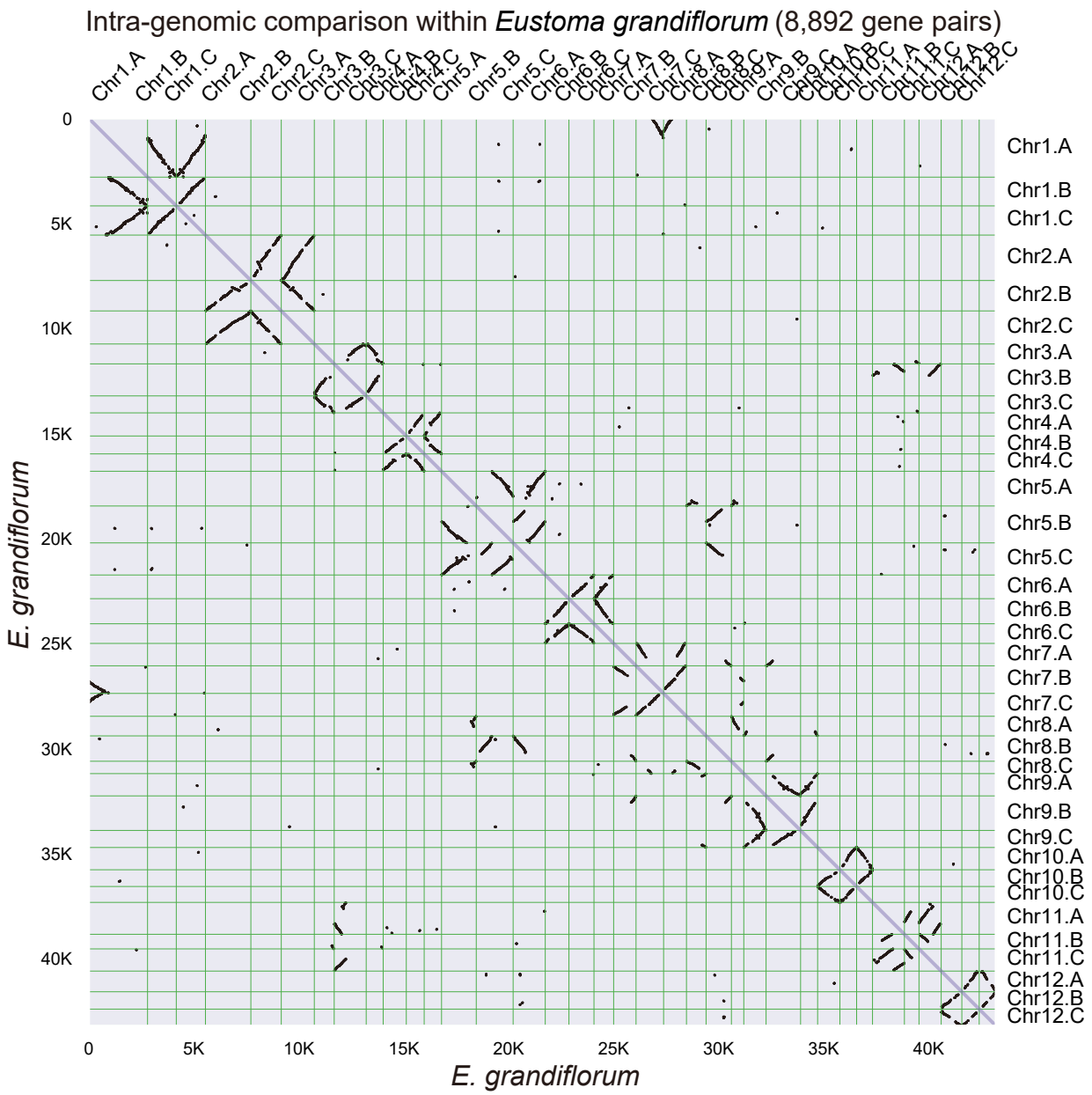

Figure S3. Dot plot of paralogues in *Eustoma grandiflorum* genome.

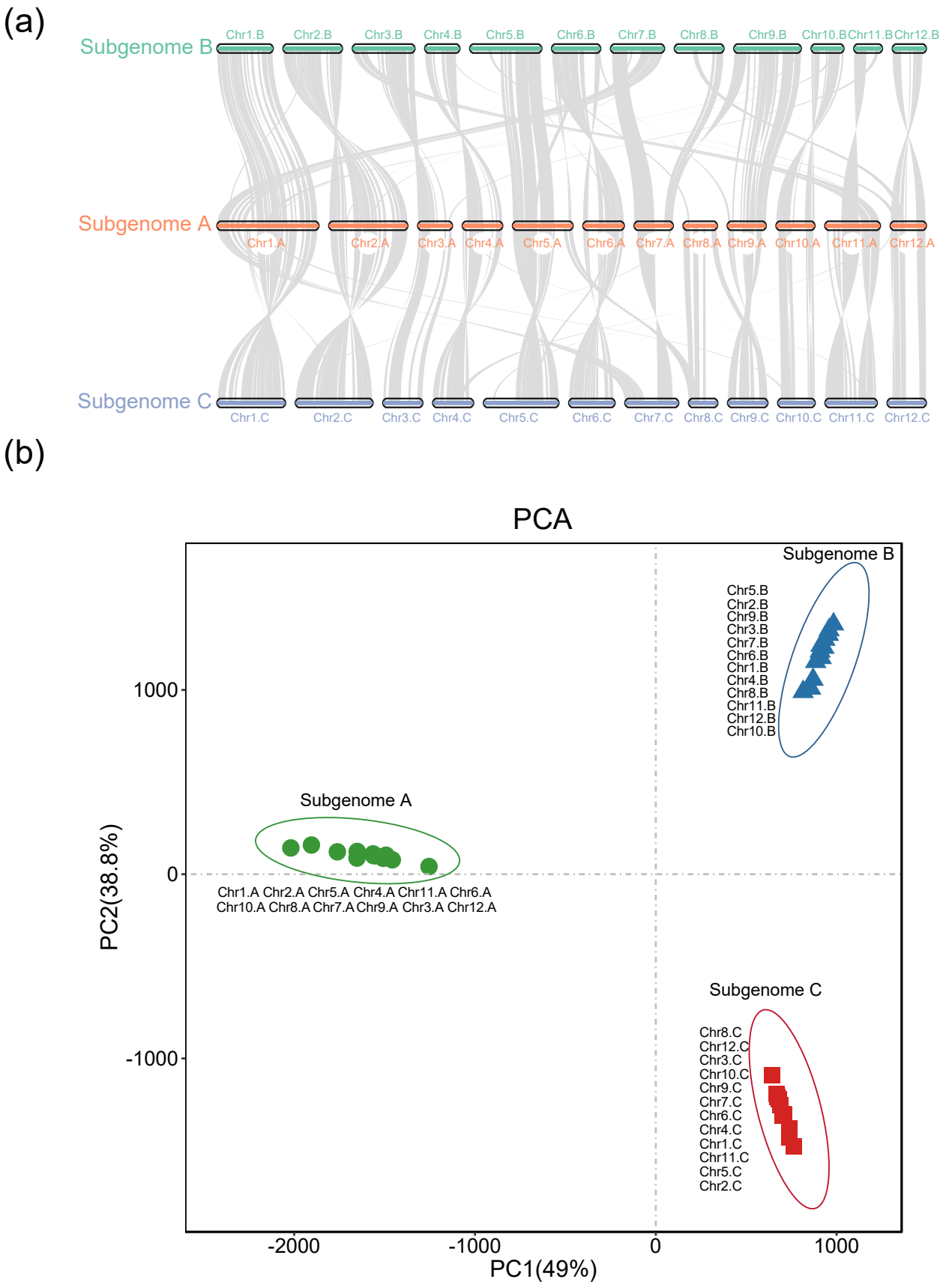

Figure S4. (a) Genomic alignments between the three sets of monoploid chromosomes (A, B, and C) in *Eustoma grandiflorum*. (b) Tracing possible origin of homologous chromosomes through principal component analysis (PCA) of transposable element profiles.

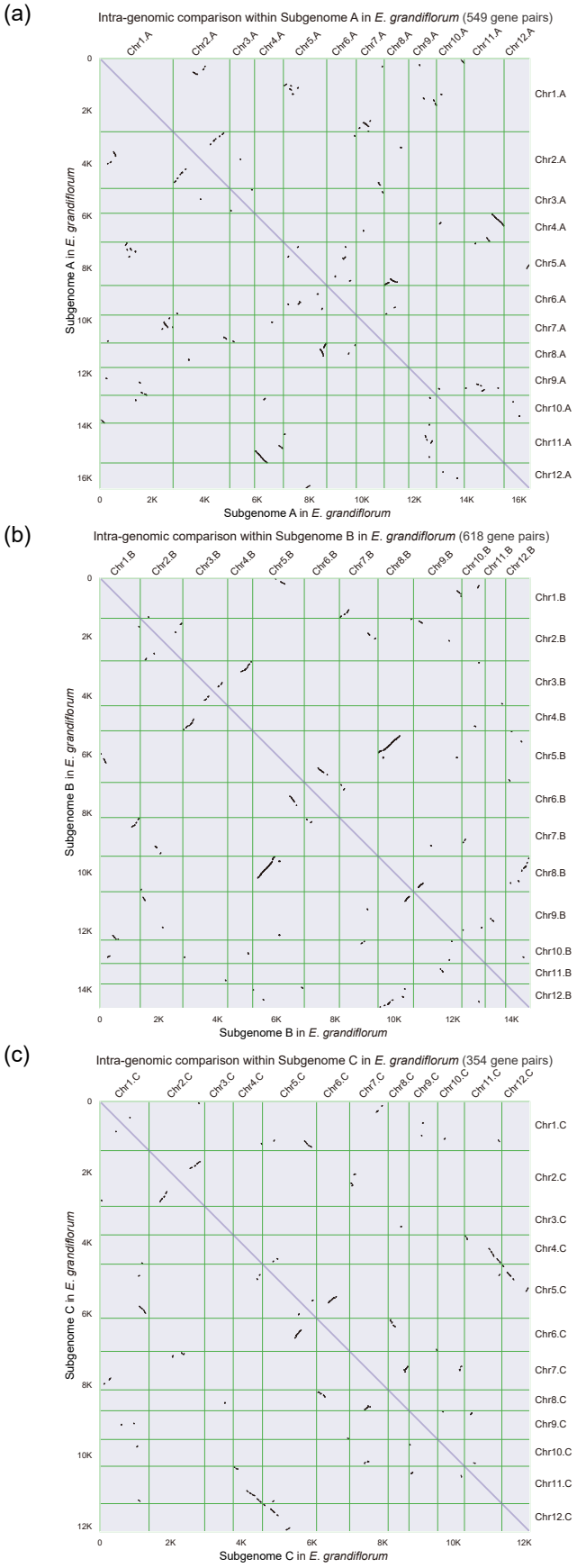

Figure S5. Dot plot of paralogues in *Eustoma grandiflorum* subgenome A (a), subgenome B (b), and subgenome C (c).

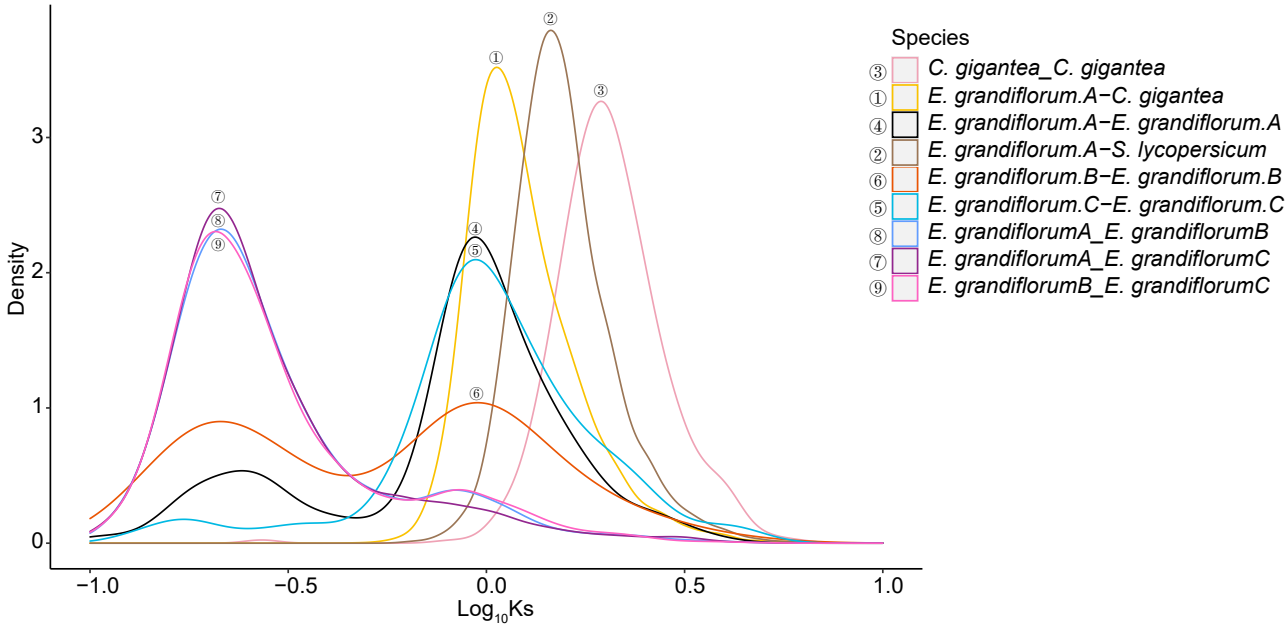

Figure S6. Ks distributions of orthologous gene pairs. Peaks 4, 5, and 6 revealed a recent species-specific WGD event during the evolution of *Eustoma grandiflorum*. Peaks 7, 8, and 9 revealed a recent species-specific WGT event during the evolution of *E. grandiflorum*. Peak 1 and 2 represent the divergence of the A set of monoploid chromosomes in *E. grandiflorum* and *Calptropis gigantea* and the A set of monoploid chromosomes in *E. grandiflorum* and *Solanum lycopersicum*, respectively.

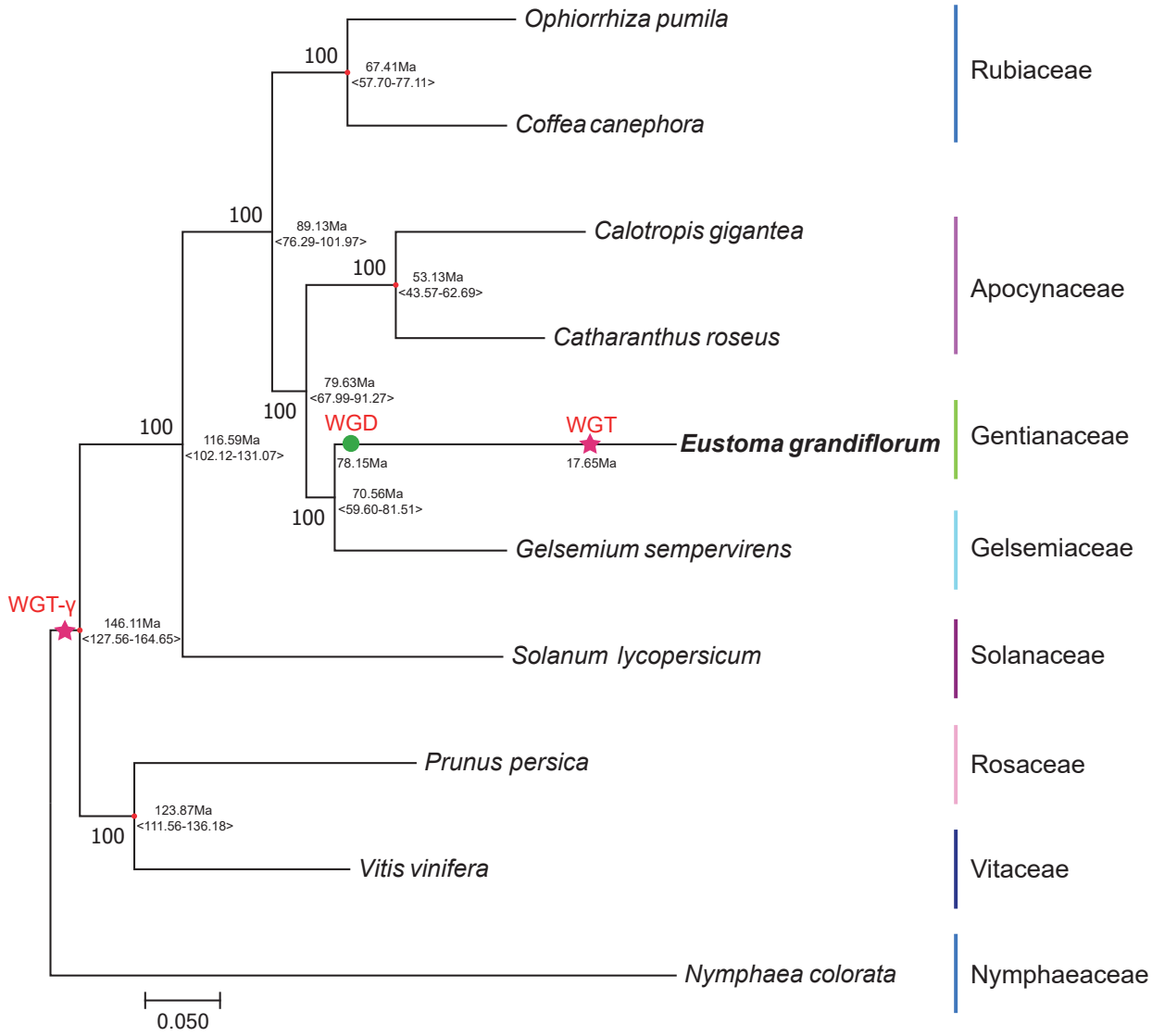

Figure S7. Phylogenetic tree showing the evolutionary relationships of *Eustoma grandiflorum* to other 9 plants. The WGT and WGD events are indicated by star and circle, respectively, along with their corresponding estimated time. The 95% HPD split time is shown above each node. Red circles represent fossil calibrations used.

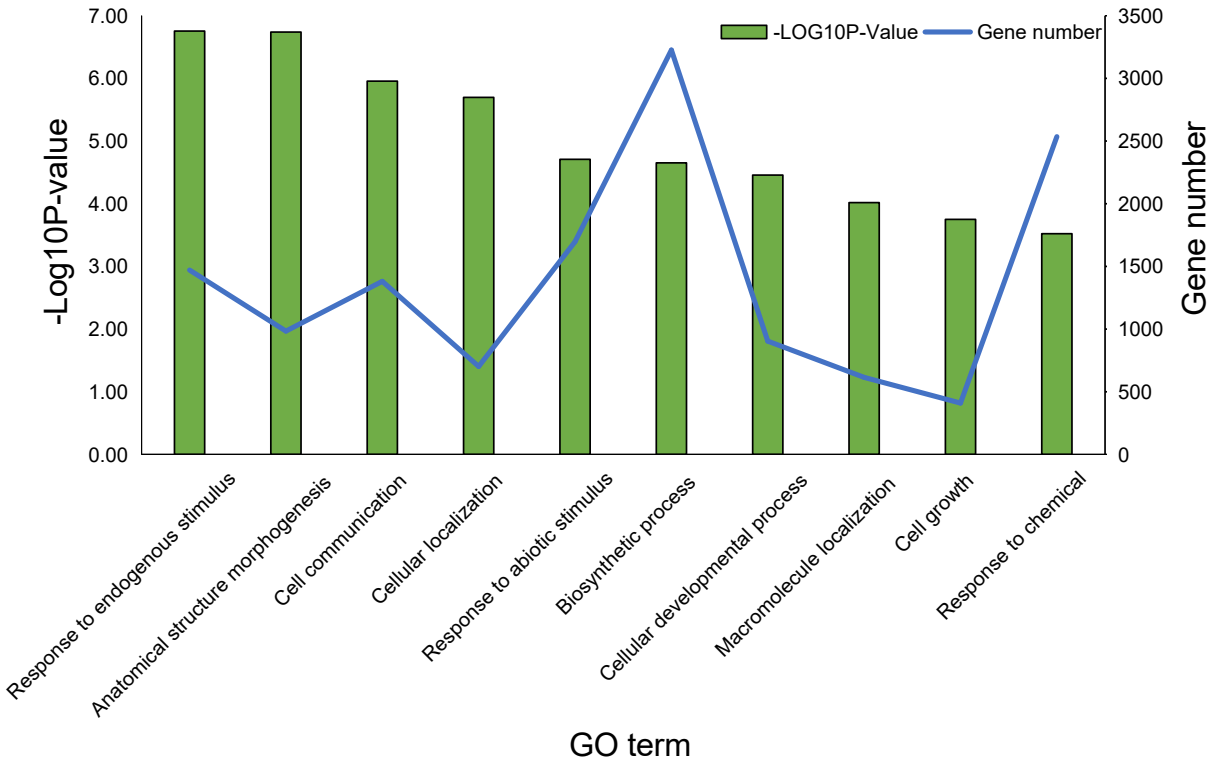

Figure S8. GO enrichment analysis of genes resulted by the WGT event.

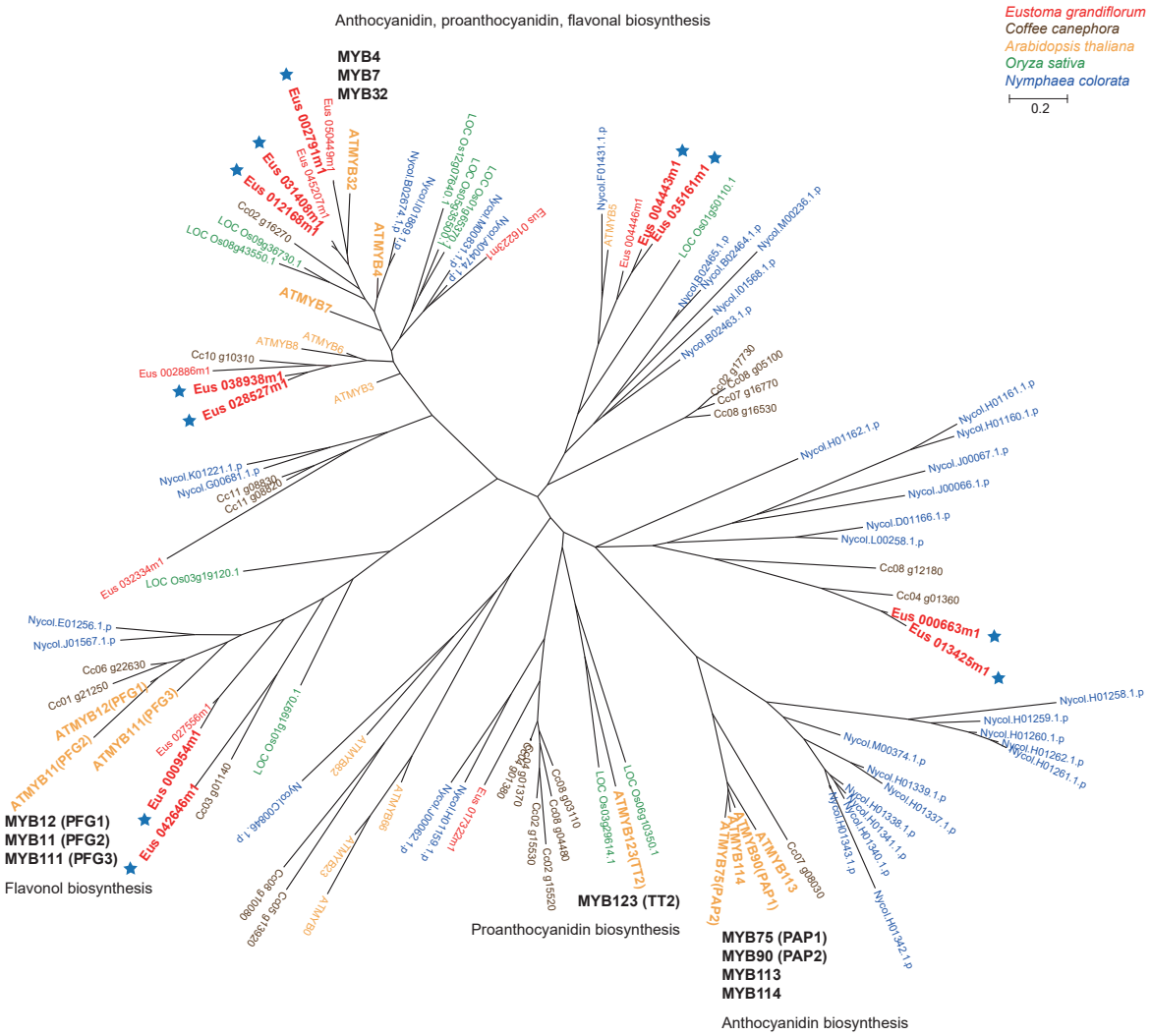

Figure S9. Phylogenetic tree of MYBs involved in flavonoid/anthocyanin biosynthesis pathways. Genes resulted by the WGT event in lisianthus are indicated by stars.

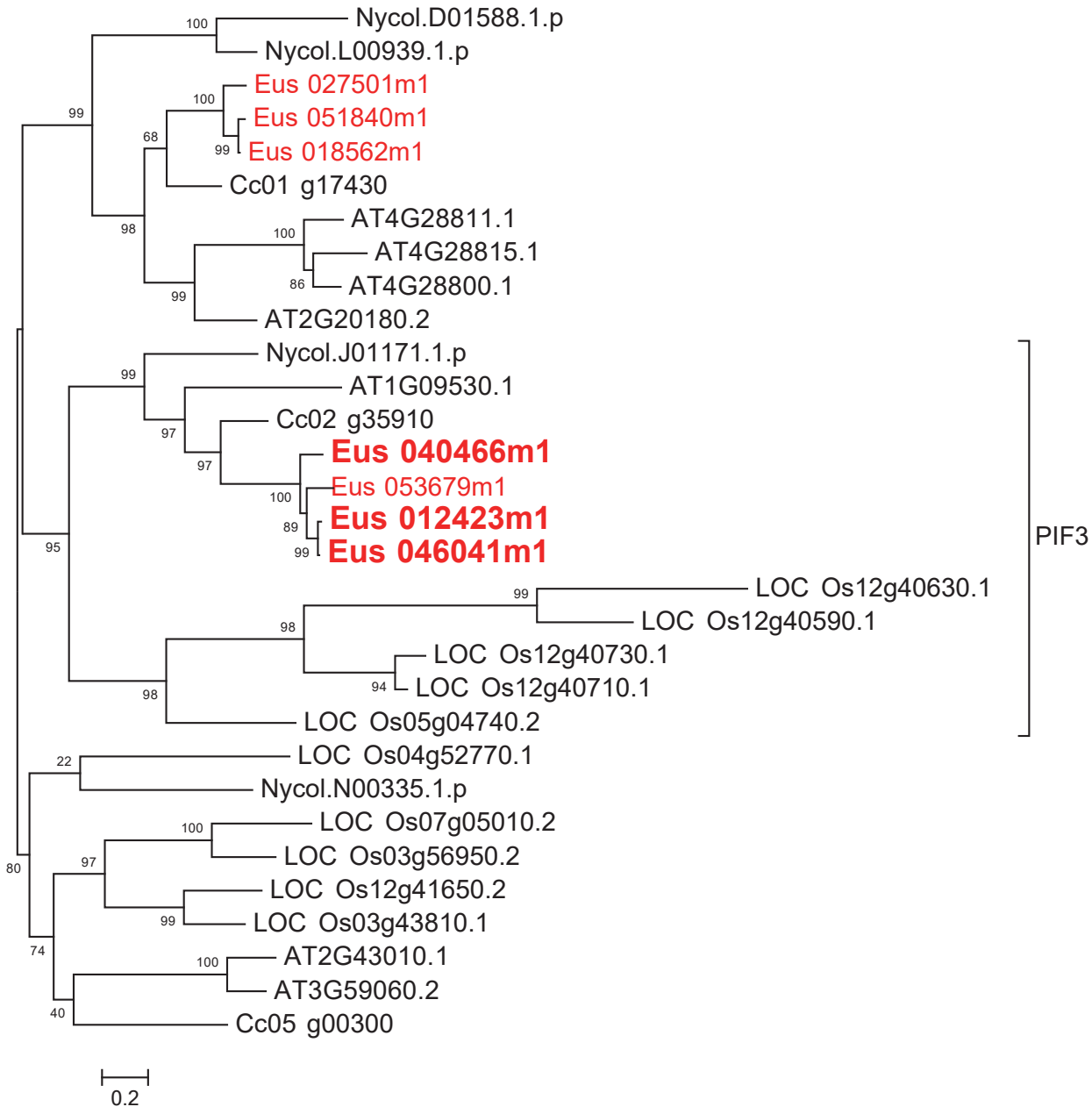

Figure S10. Phylogenetic tree of PIF genes in the bHLH family. Genes resulted by the WGT event in lisianthus are in red bold fonts.

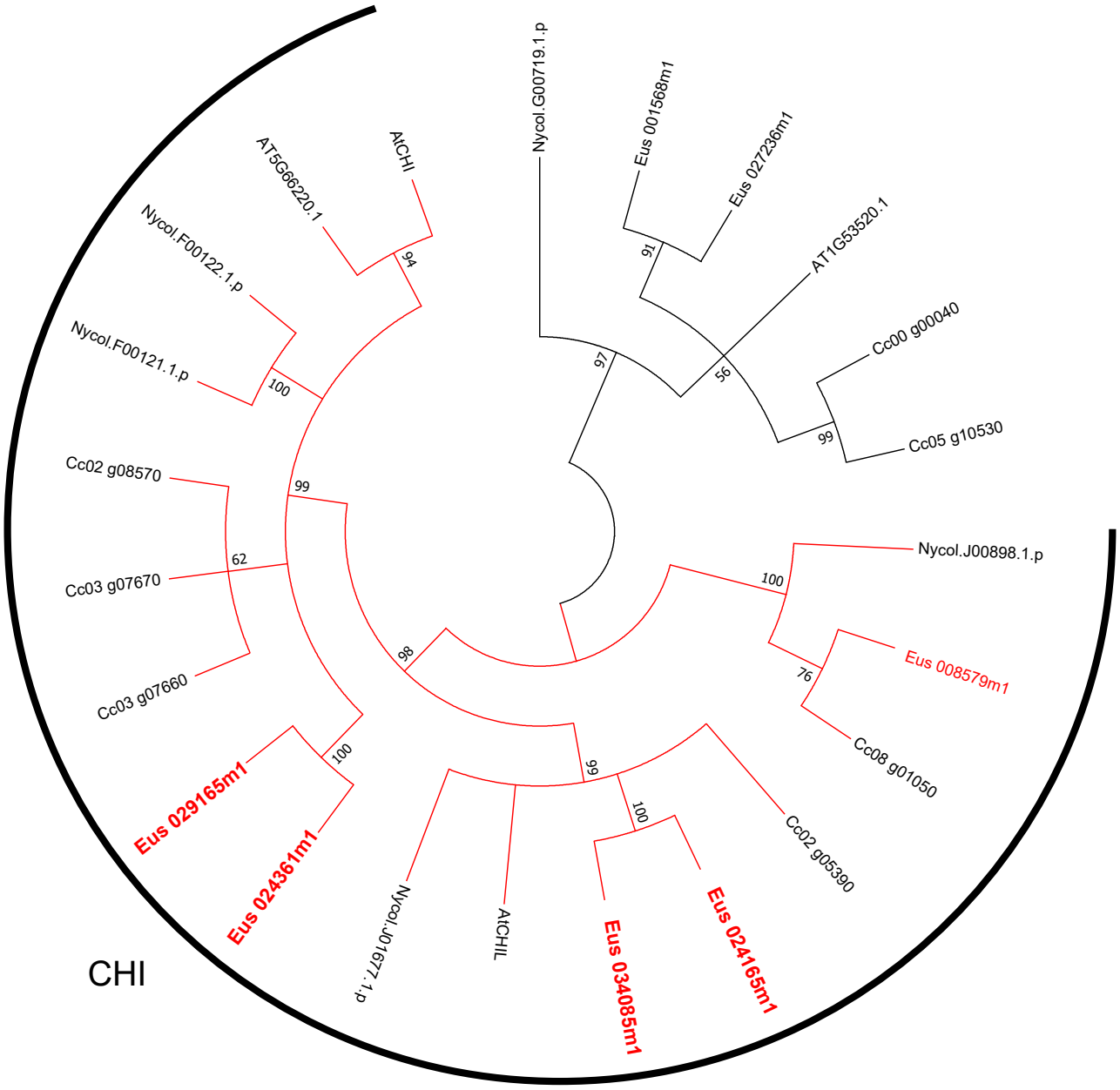

Figure S11. Phylogenetic tree of CHIs. Genes with synteny genes resulted by the polyploidy event in lisianthus are in red bold fonts.

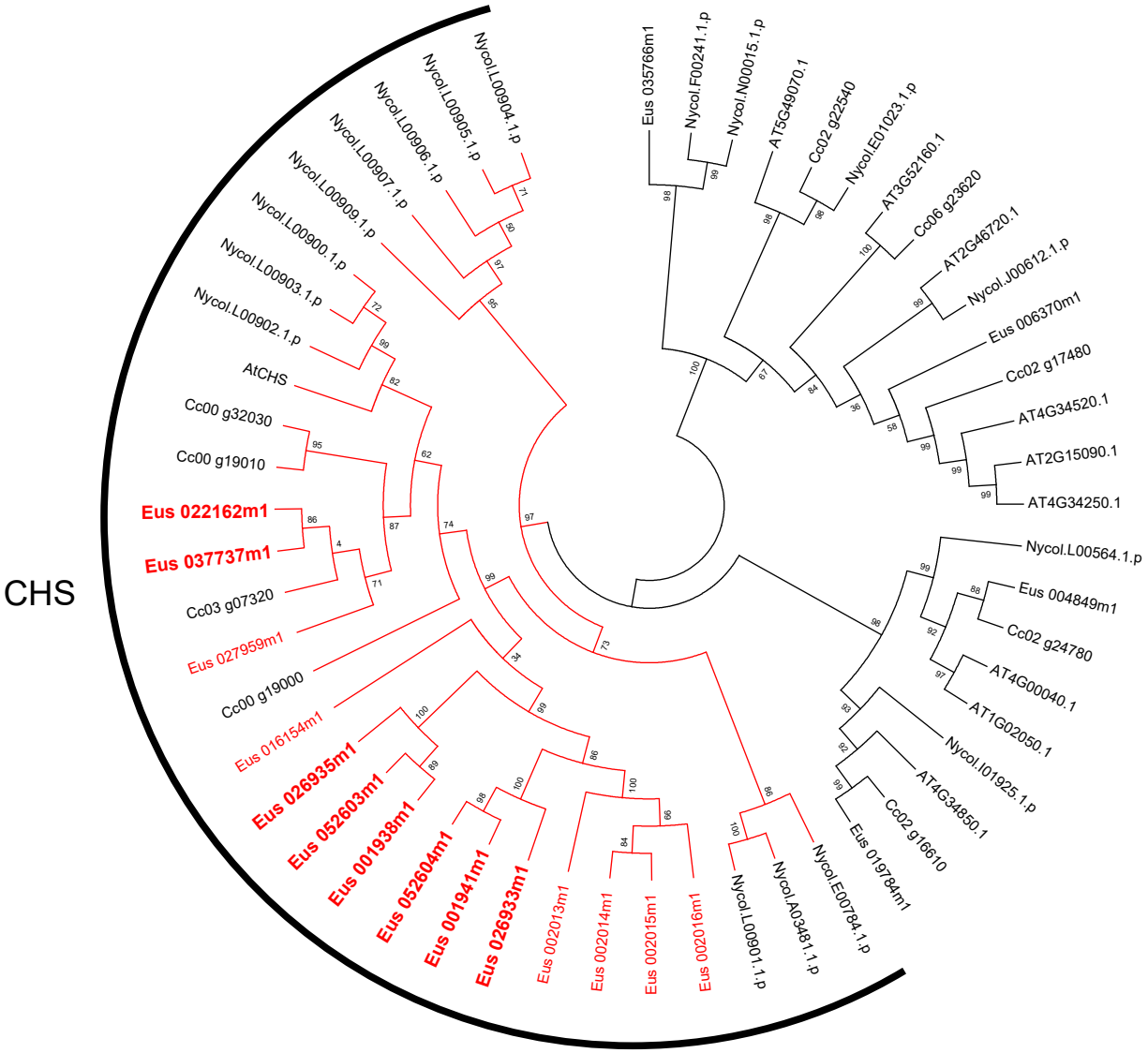

Figure S12. Phylogenetic tree of CHSs. Genes resulted by the WGT event in lisianthus are in red bold fonts.

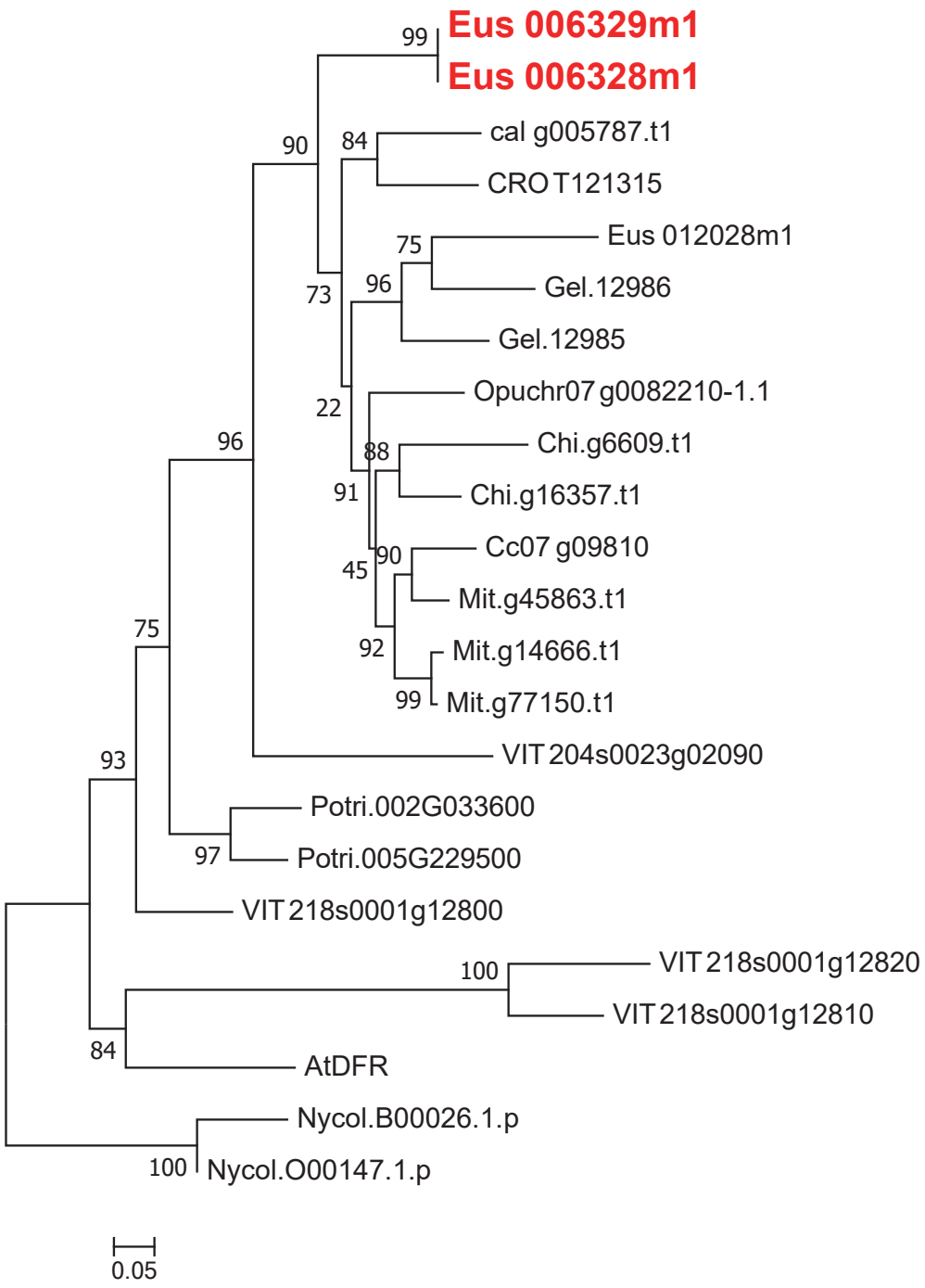

Figure S13. Phylogenetic tree of DFRs. Genes resulted by the WGT event in lisianthus are in red bold fonts.

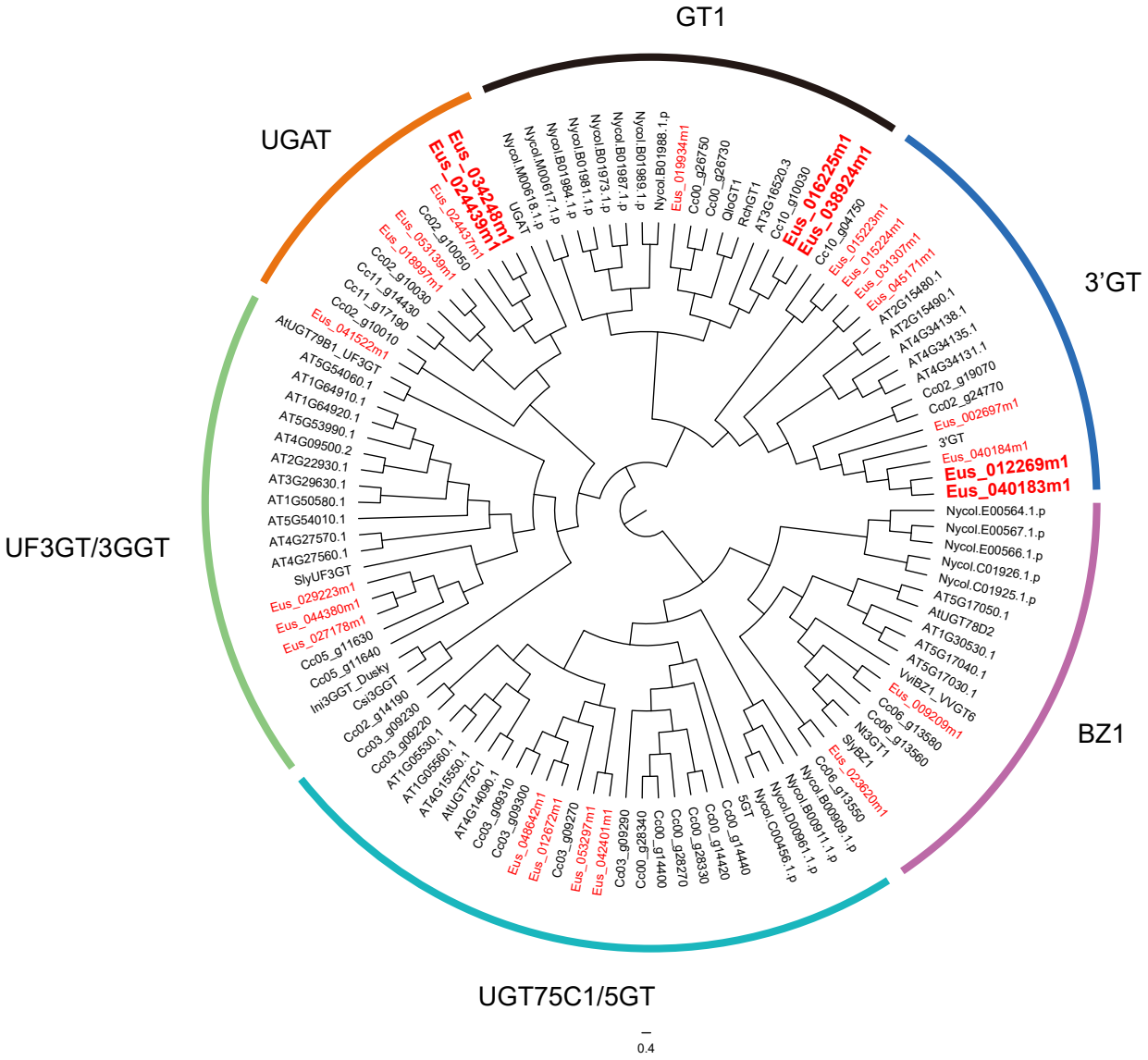

Figure S14. Phylogenetic tree of UDPGTs involved in anthocyanin biosynthesis. Genes resulted by the WGT event in lisianthus are in red bold fonts.

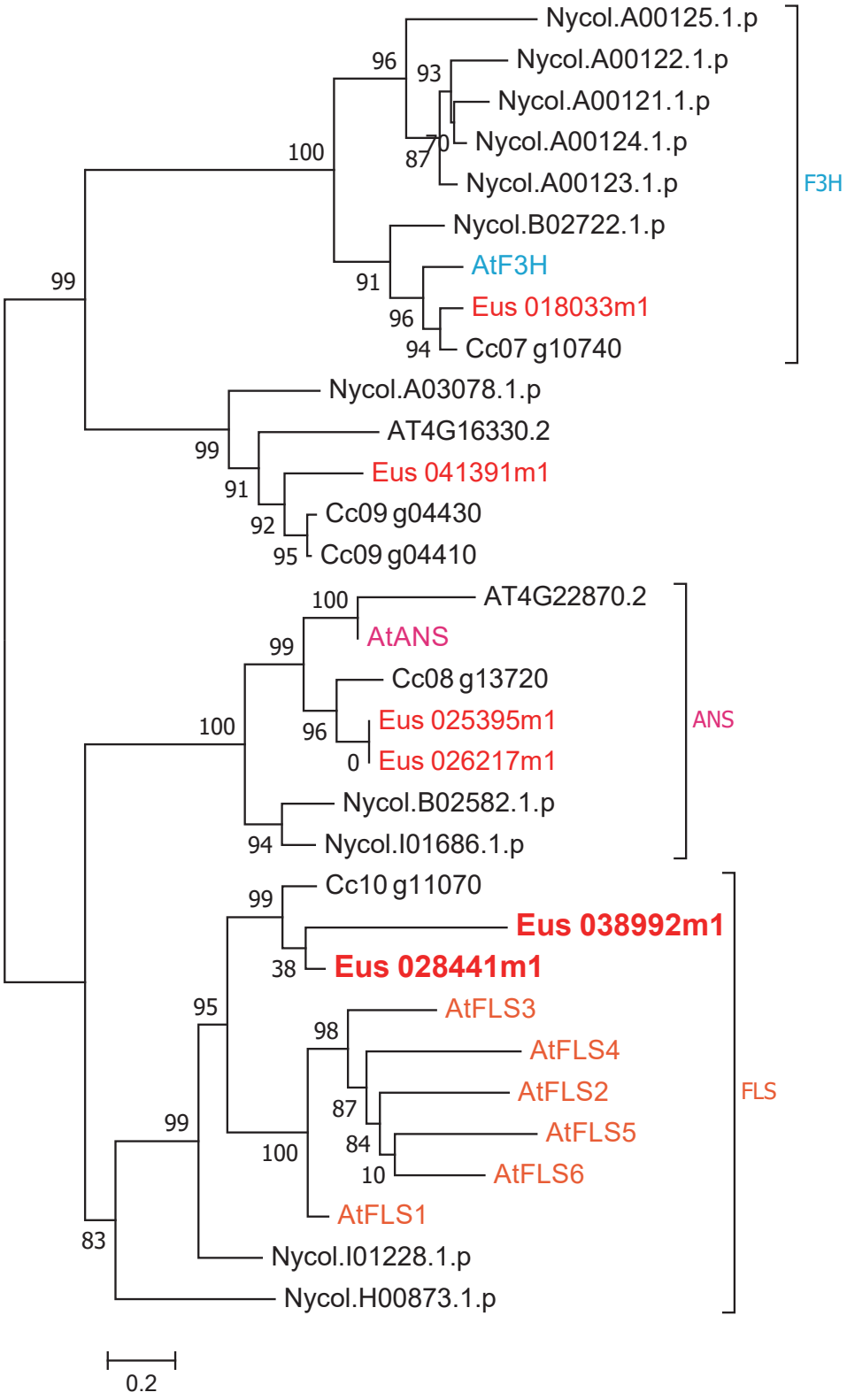

Figure S15. Phylogenetic tree of F3Hs, ANSs, and FLSs. Genes resulted by the WGT event in lisianthus are in red bold fonts.

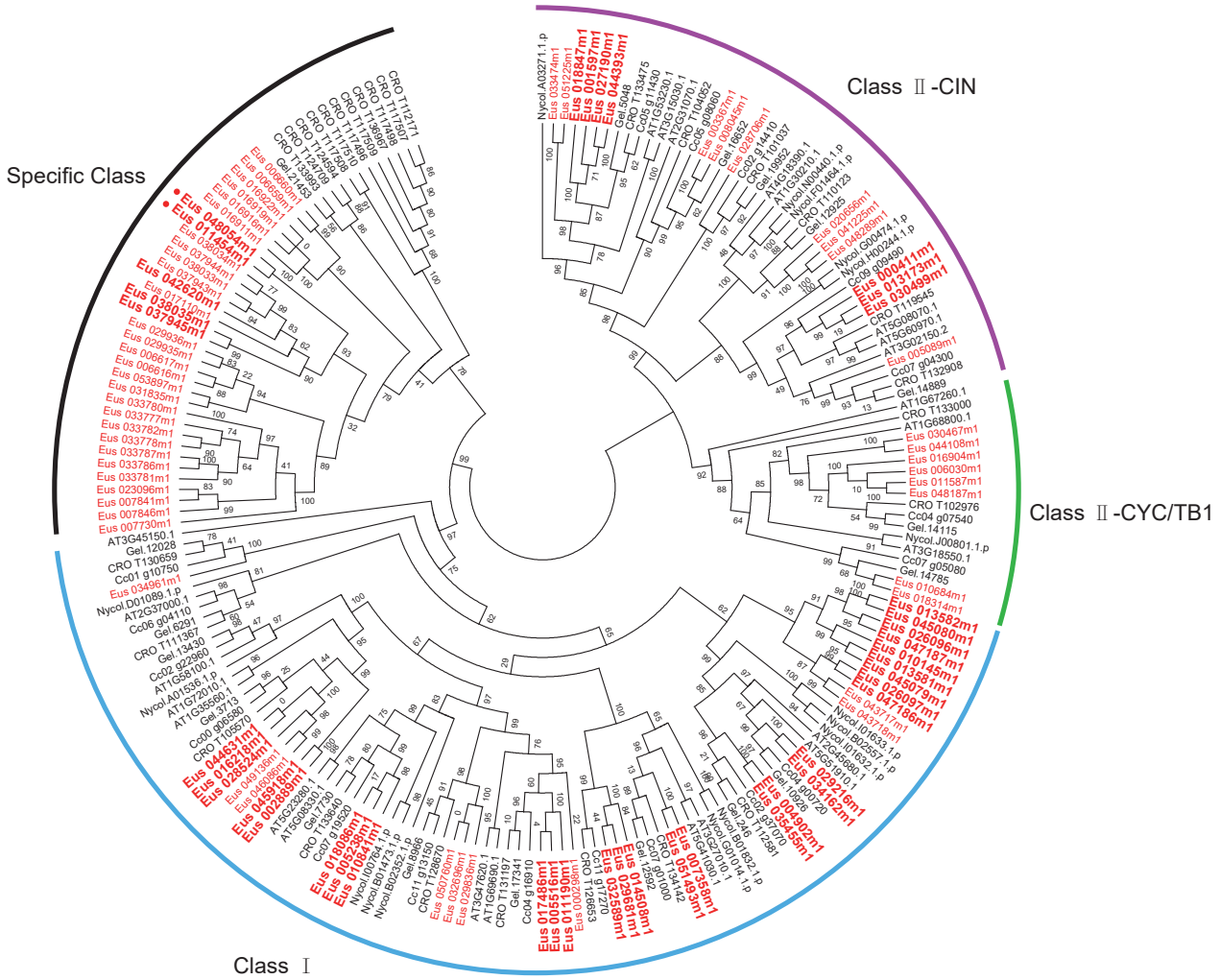

Figure S16. Phylogenetic tree of TCPs. Genes resulted by the WGT event in lisianthus are indicated by red bold fonts without circles, genes resulted by the WGD event in lisianthus are indicated by red bold fonts with circles.

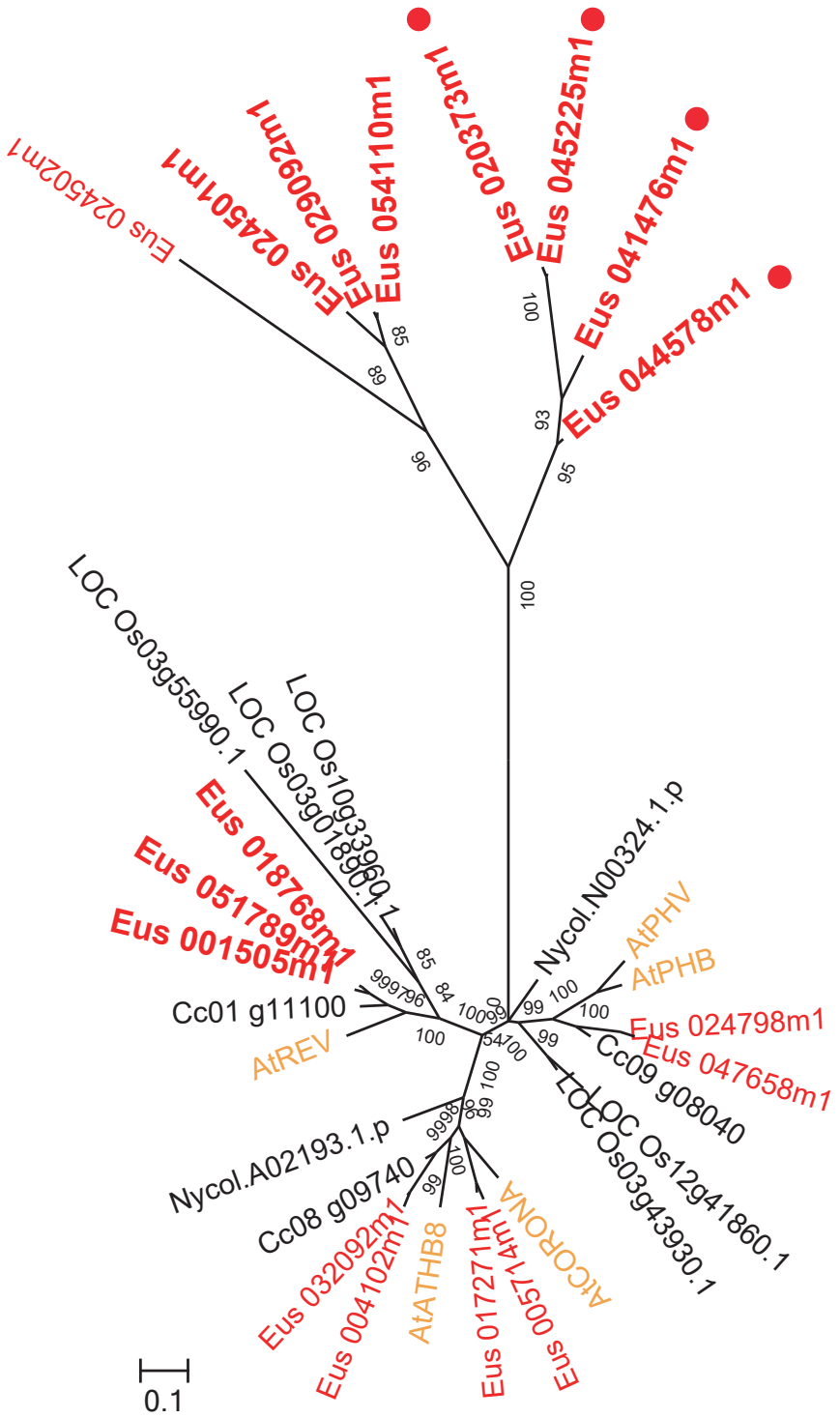

Figure S17. Phylogenetic tree of members in the HD-Zip III family. Genes with synteny genes resulted by the polyploidy WGT event in lisianthus are indicated by red bold fonts without circles, genes resulted by the WGD event in lisianthus are indicated by red bold fonts with circles.

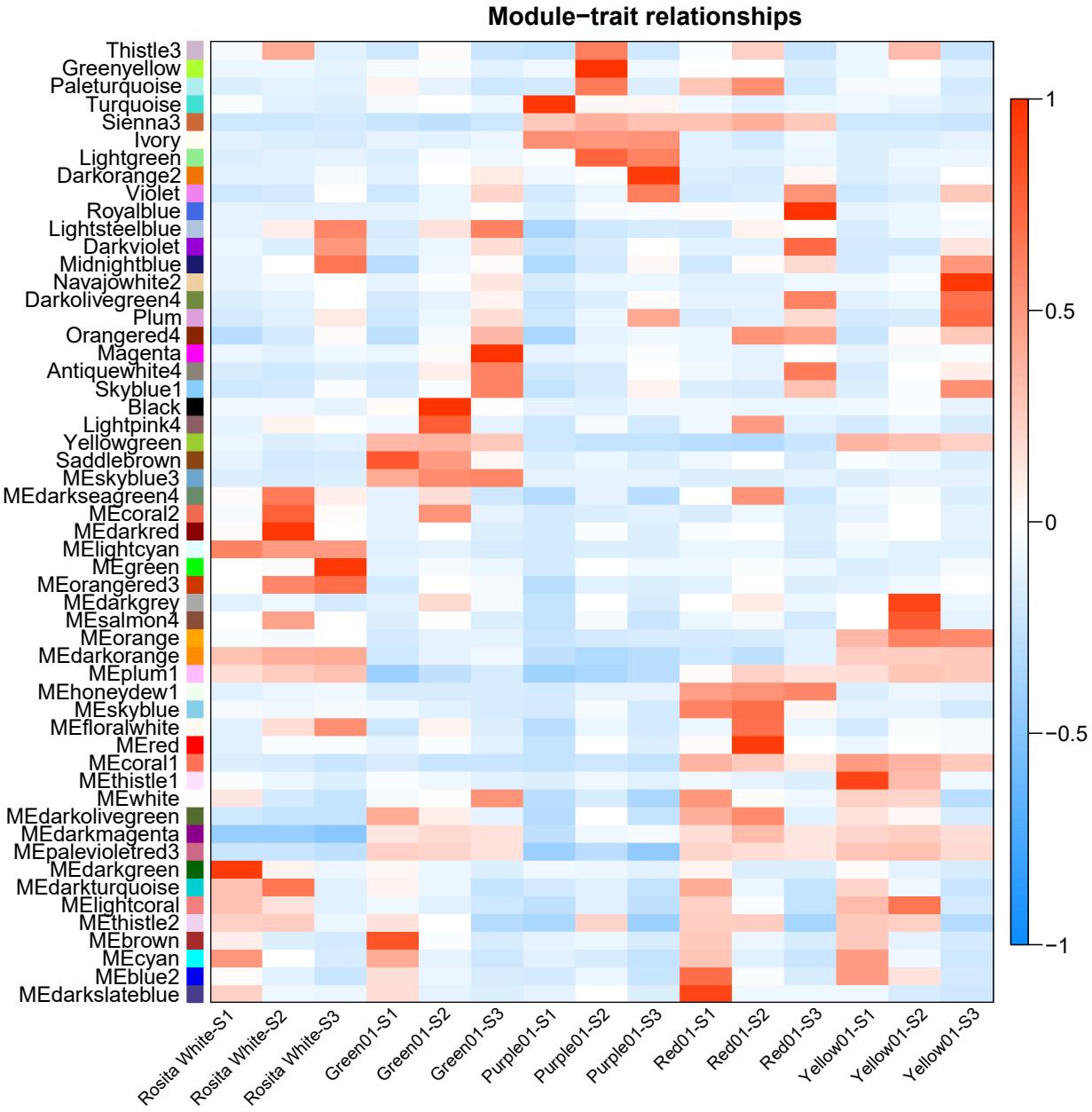

Figure S18. Module-tissue association in different lisianthus cultivars. Each row corresponds to a module. Each column corresponds to a specific sample. The color of each cell at the row-column intersection indicates the correlation coefficient between the module and the trait. The bud stage, S1; the turning stage, S2; the blooming stage, S3.

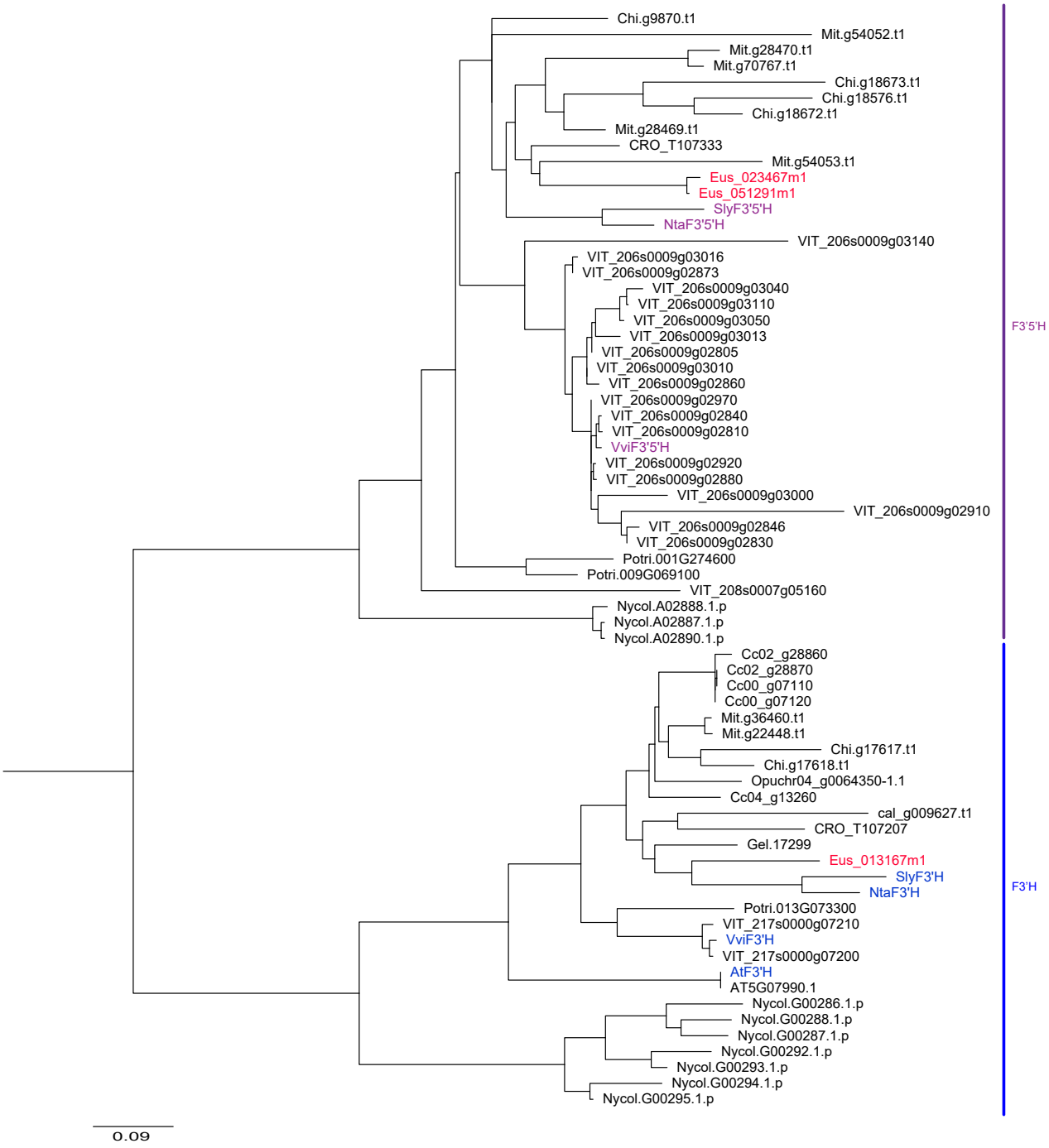

Figure S19. Phylogenetic tree of F3'Hs and F3'5'Hs.

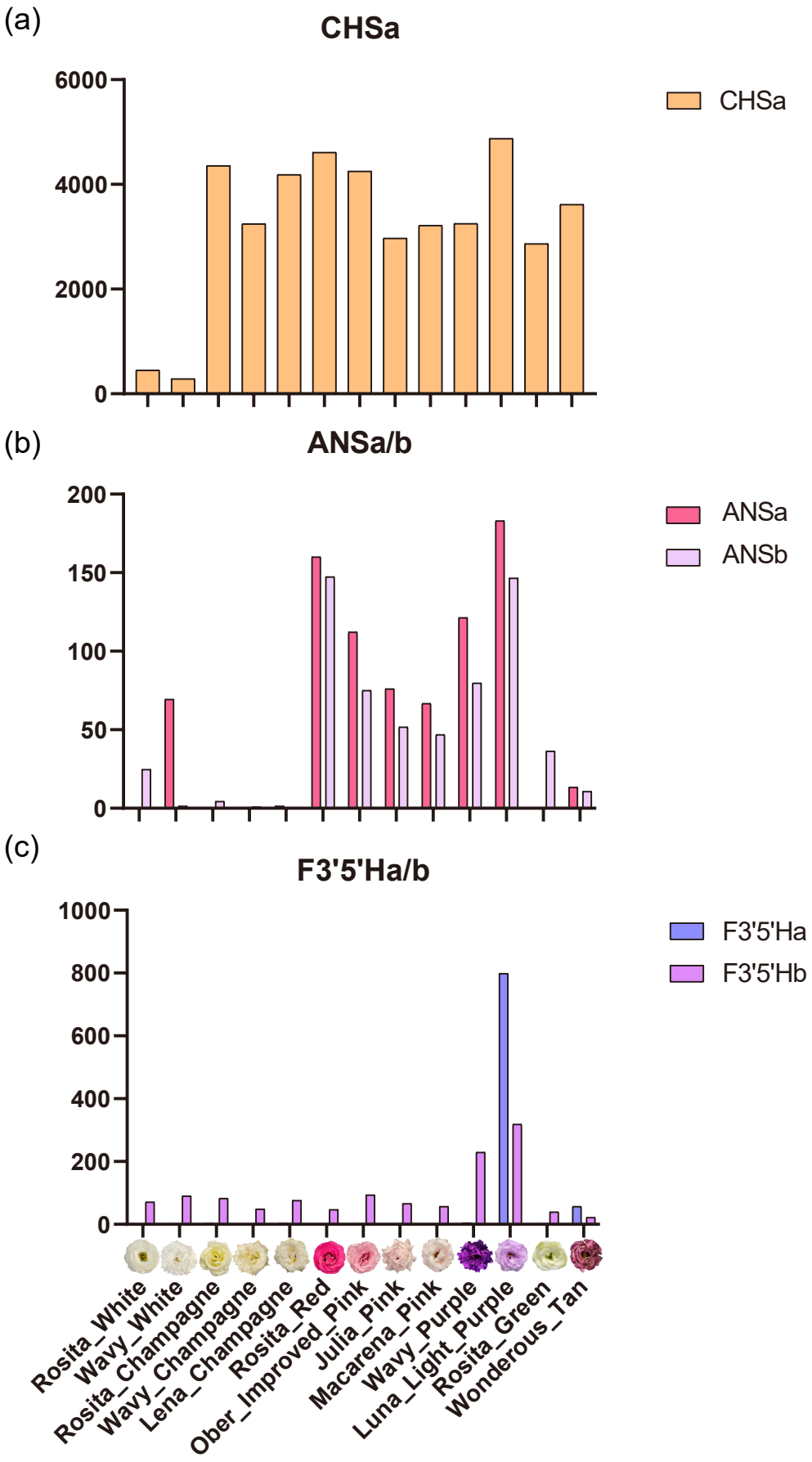

Figure S20. Histograms showing expression levels (FPKM) of important regulatory genes involved in anthocyanin biosynthesis in different lisianthus varieties during development, including CHSa (a), ANSA/b (b), and F3’5’Ha/b (c). Bud stage, S1; turning stage, S2; blooming stage, S3.

(a)

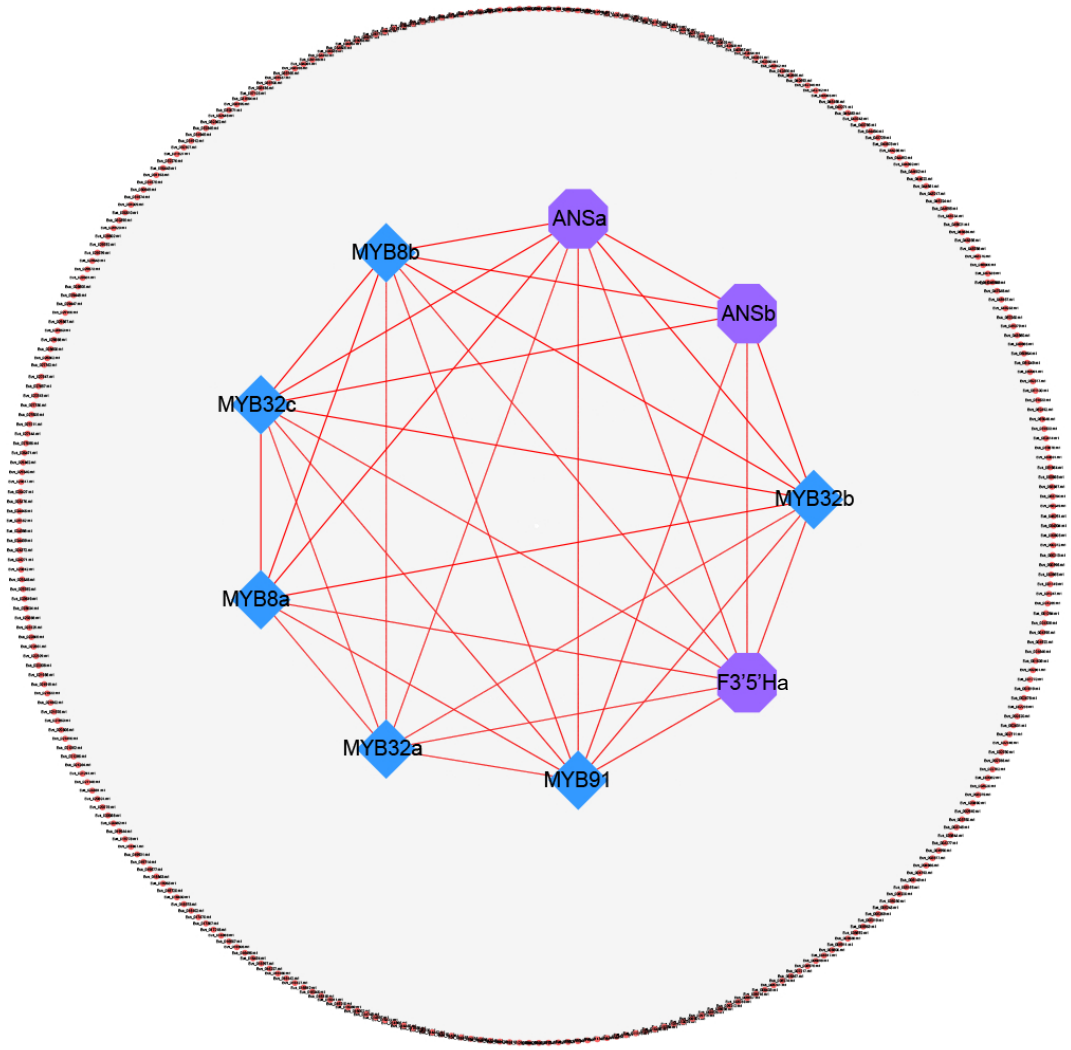

(b)

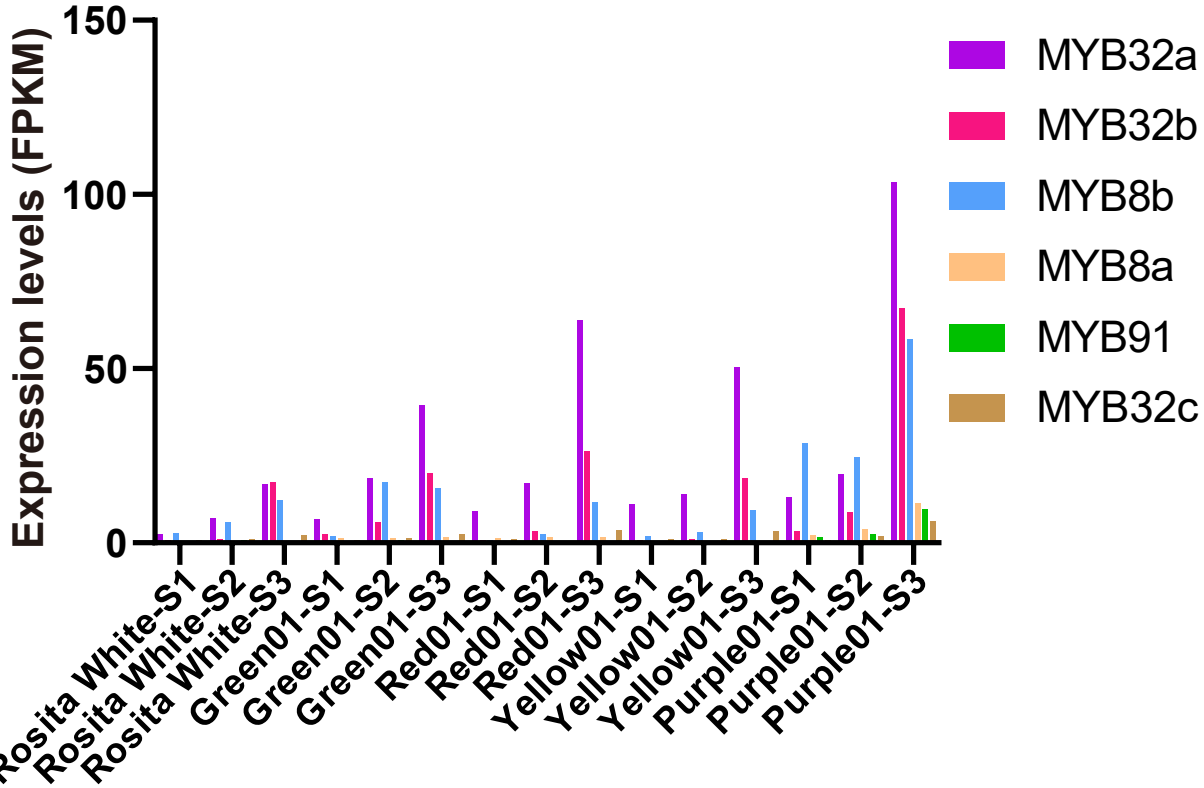

Figure S21. (a) Co-expression network of the "darkorange2" module. (b) Histograms showing expression levels (FPKM) of MYB genes in the "darkorange2" module. S1, bud stage; S2, turning s tage; S3, blooming stage.

Figure S22. Phylogenetic tree of Chlorophyll a/b-binding (CAB) protein family. Genes in *Eustoma grandiflorum and Arabidopsis thaliana* are in red fonts and yellow fonts, respectively.

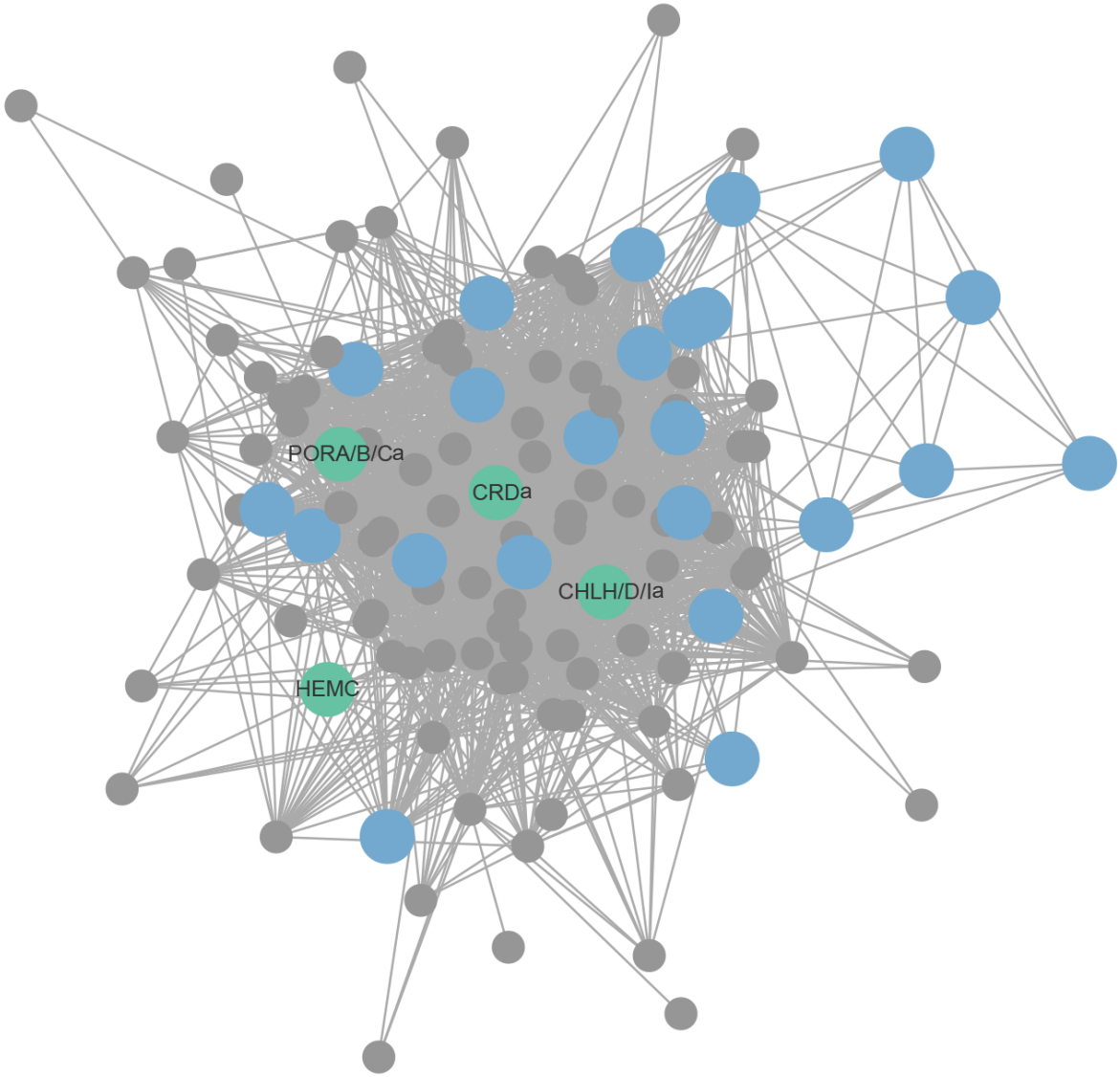

Figure S23. Co-expressed network of the white module correlated with S3 in Green01. Blue nodes display Chlorophyll a/b-binding proteins.

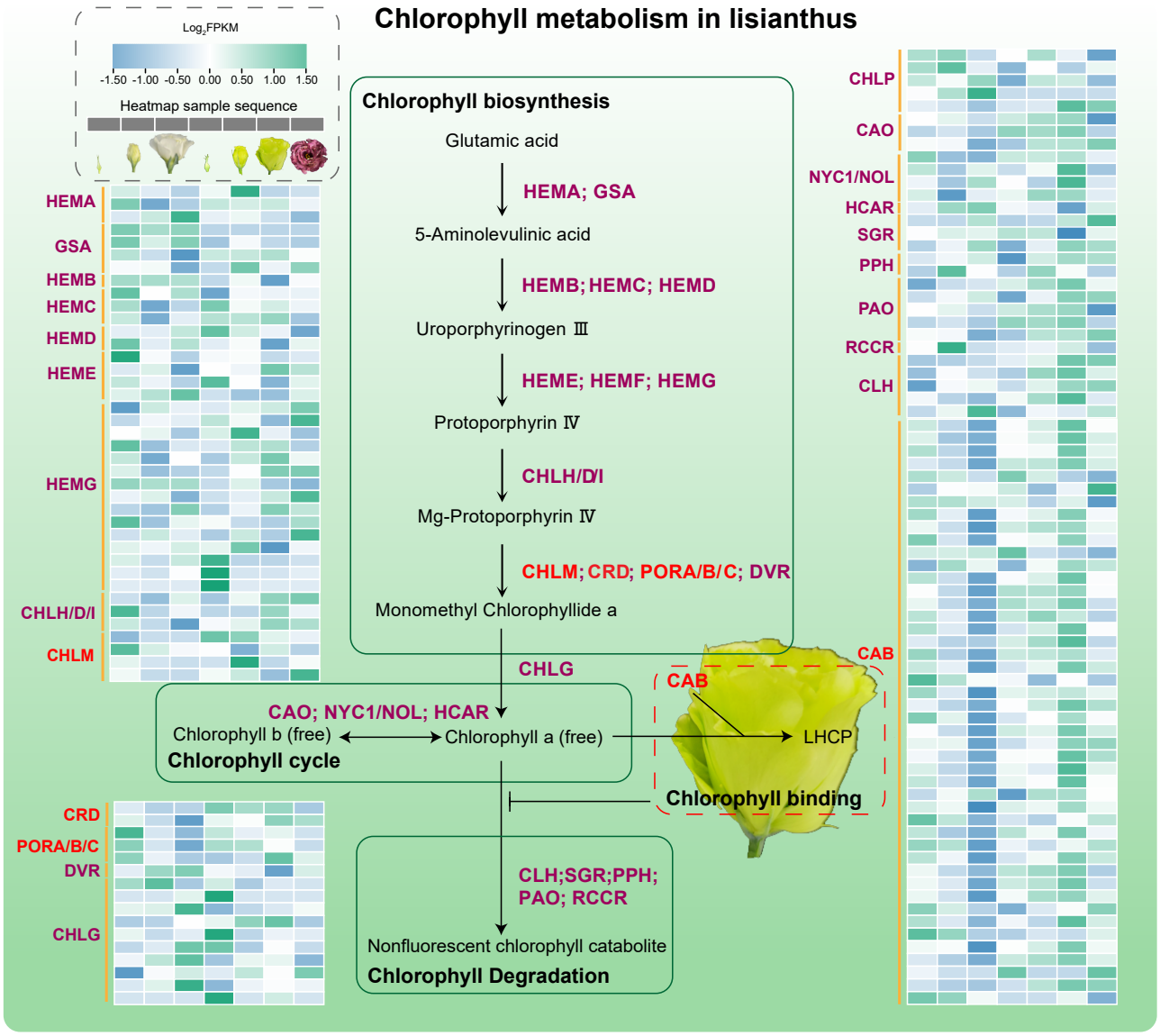

Figure S24. The potential chlorophyll metabolic pathway in petals in *Eustoma grandiflorum*. The chlorophyll metabolic pathway is classified into four distinct parts: chlorophyll biosynthesis, chlorophyll cycle, chlorophyll binding, and chlorophyll degradation. HEMA, glutamyl-tRNA reductase; GSA, glutamate-1-semialdehyde 2,1-aminomutase; HEMB, 5-aminolevulinate dehydratase; HEMC, hydroxymethylbilane synthase; HEMD, uroporphyrinogen III synthase; HEME, uroporphyrinogen III decarboxylase; HEMF, coproporphyrinogen III oxidase; HEMG, protoporphyrinogen IX oxidase; CHLH, Mg chelatase H subunit; CHLI, Mg chelatase I subunit; CHLD, Mg chelatase D subunit; CHLM, Mg-proto IX methyltransferase; CRD, Mg-proto IX monomethylester cyclase; PORA/B/C, protochlorophyllide reductase; DVR, divinyl-protochlorophyllide reductase; CHLG, chlorophyll synthase; CAO, chlorophyllide a oxygenase; NYC1/NOL, chlorophyll b reductase; HCAR, hydroxymethyl chlorophyll a reductase; CLH, chlorophyllase; SGR, magnesium dechelatase; PPH, pheophytinase; PAO, pheophorbide a oxygenase; RCCR, red chlorophyll catabolite reductase; CAB, Chlorophyll a/b-binding protein; LHCP, light-harvesting chlorophyll a/b binding protein complex/antenna complex. Gene expression levels are presented in heatmaps next to the gene names. The bar represents the expression. Essential regulators are in red fonts.

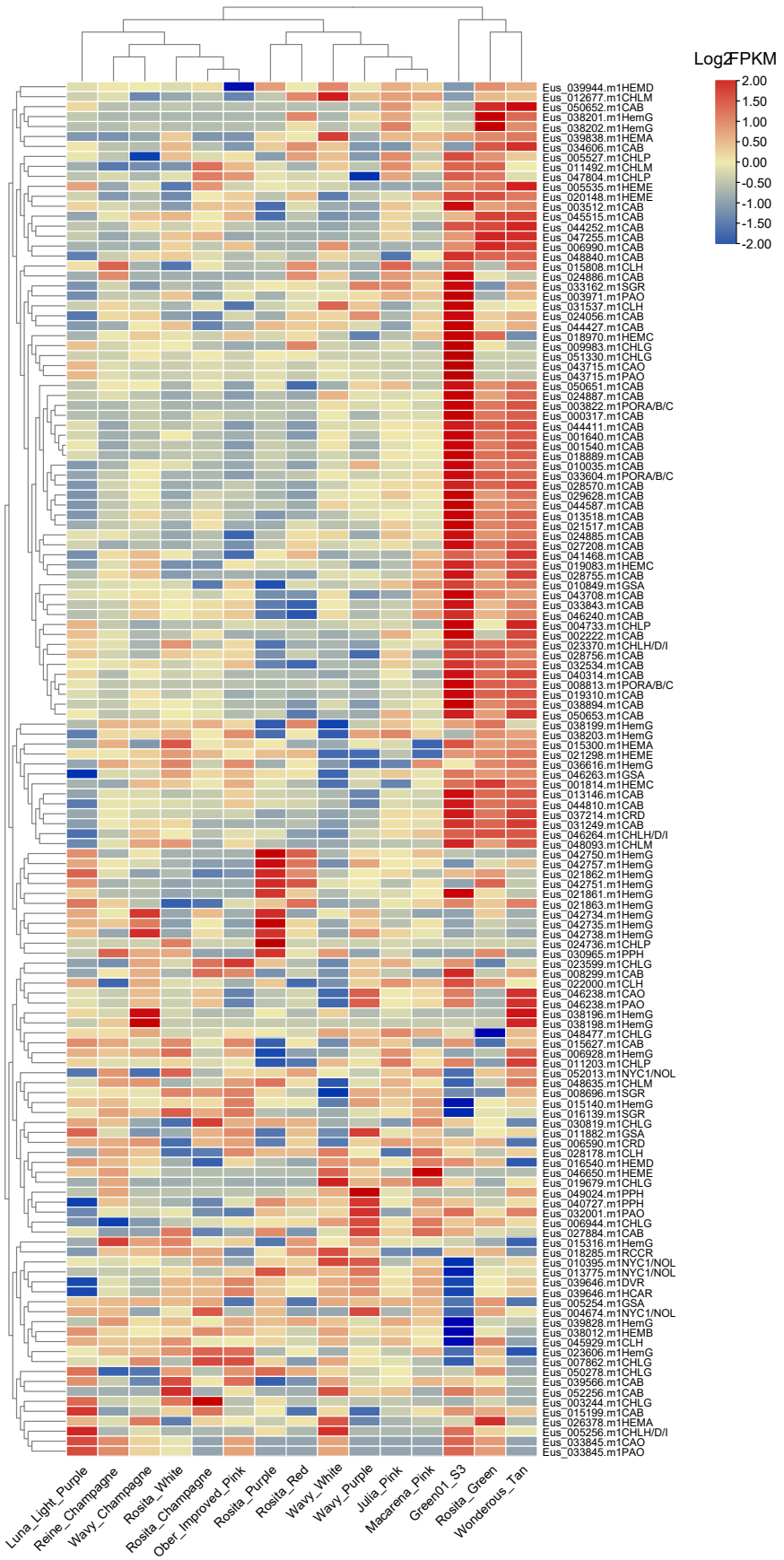

Figure S25. Heatmap showing the expression patterns of the genes involved in chlorophyll metabolism and genes in the Chlorophyll a/b-binding protein (CAB) family across different lisianthus cultivars.

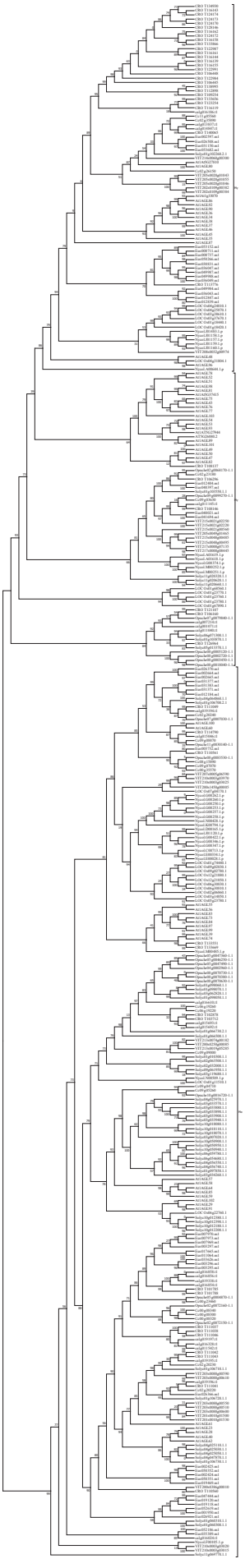

Figure S26. Phylogenetic tree of type I MADS-box genes.

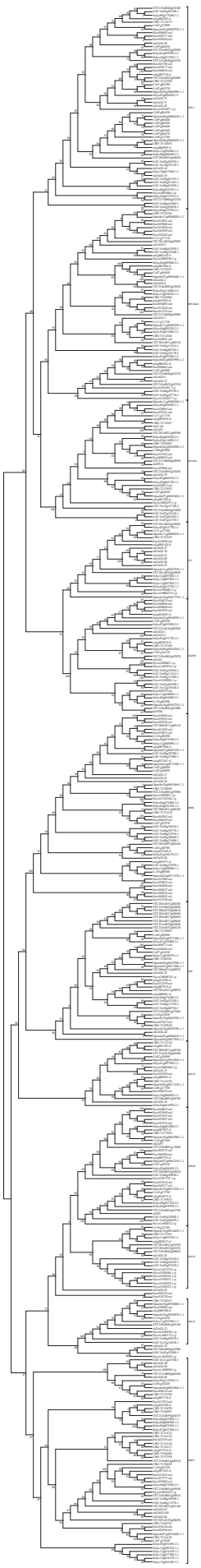

Figure S27. Phylogenetic tree of type II MADS-box genes.

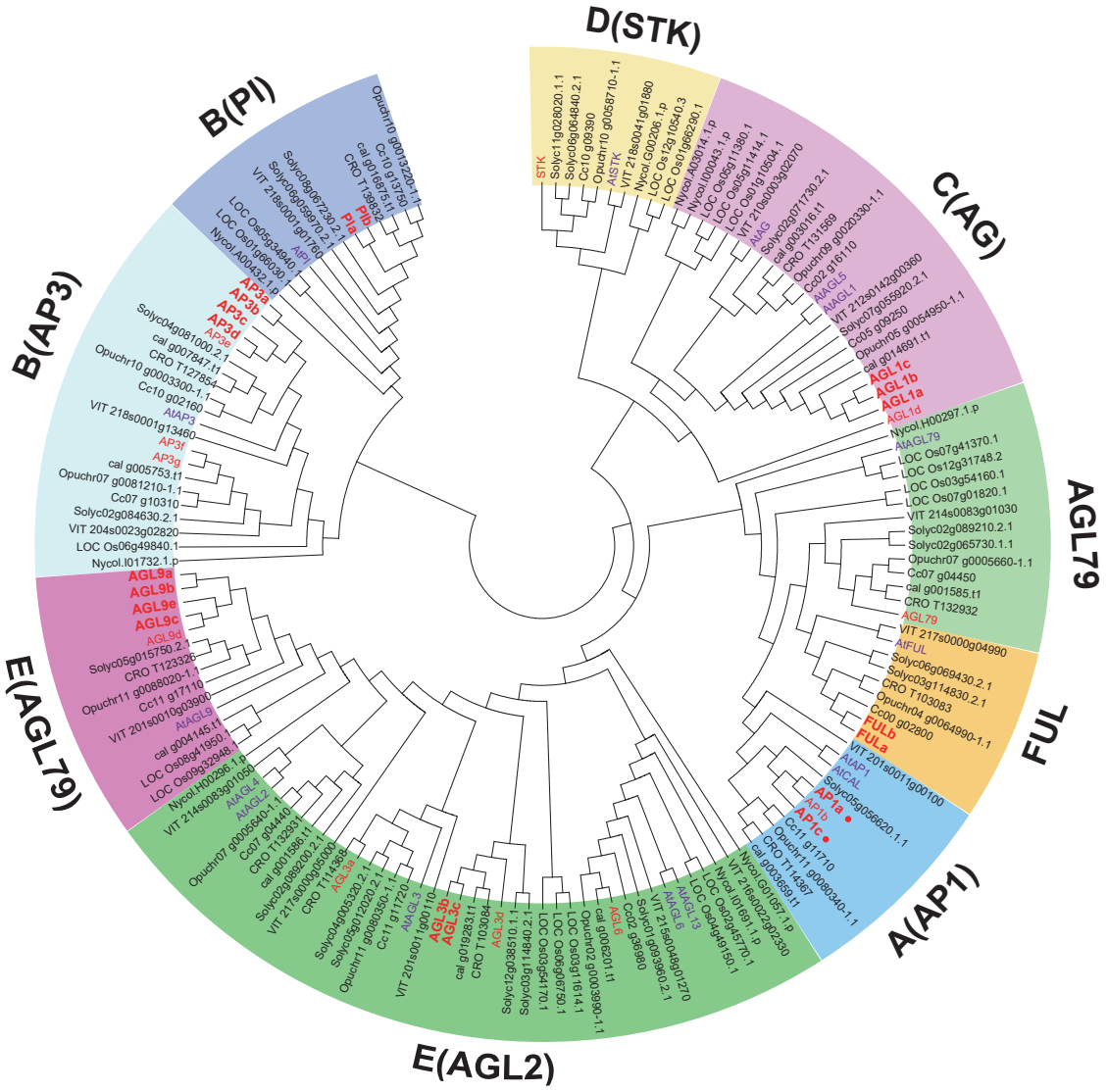

Figure S28. Phylogenetic tree of floral organ identity genes.

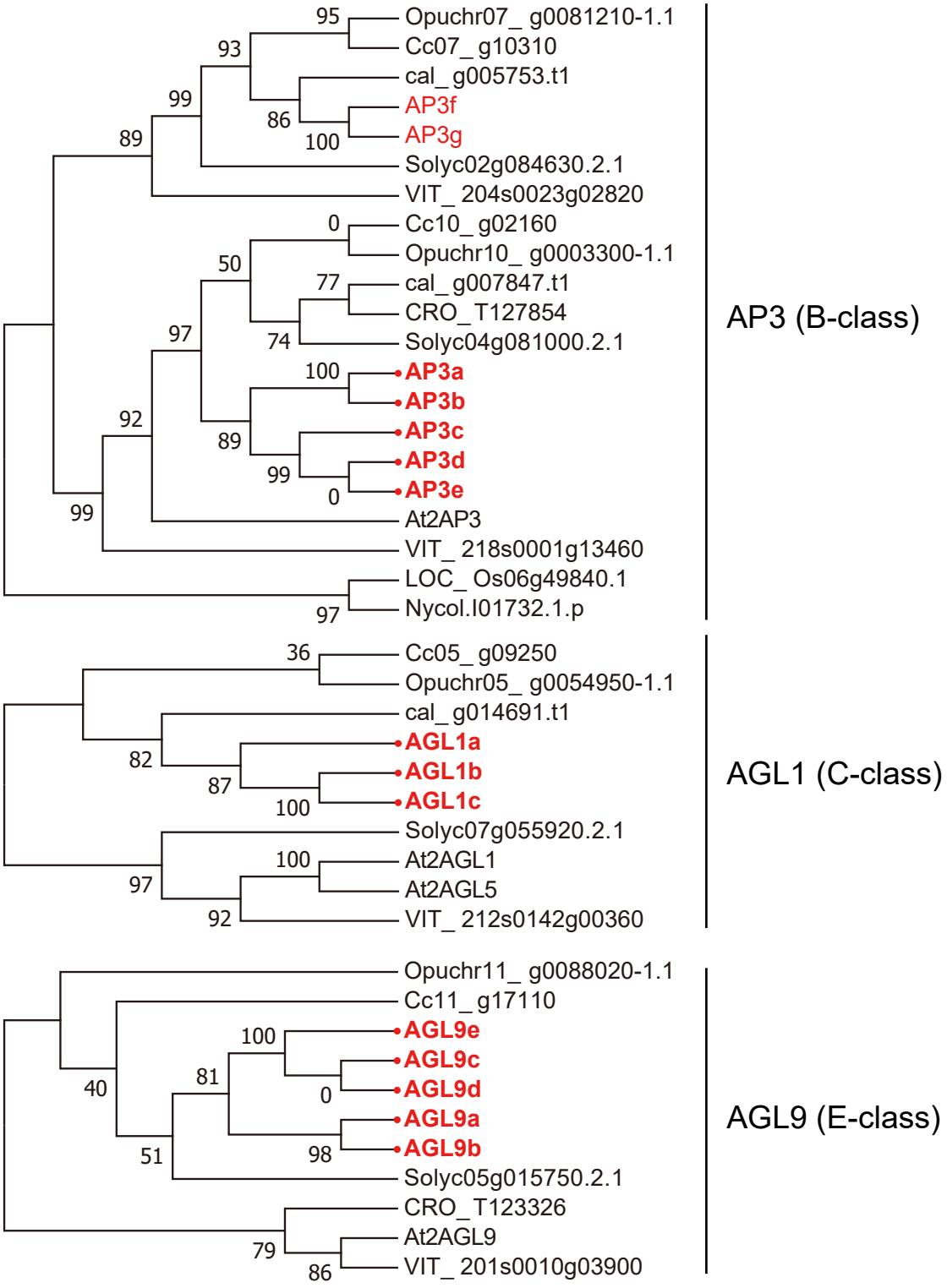

Figure S29. Phylogenetic tree of AP3 (a), AGL1(b), and AGL9 (c). Genes generated by WGT in *Eustoma grandiflorum* are indicated by red bold fonts with circle nodes.

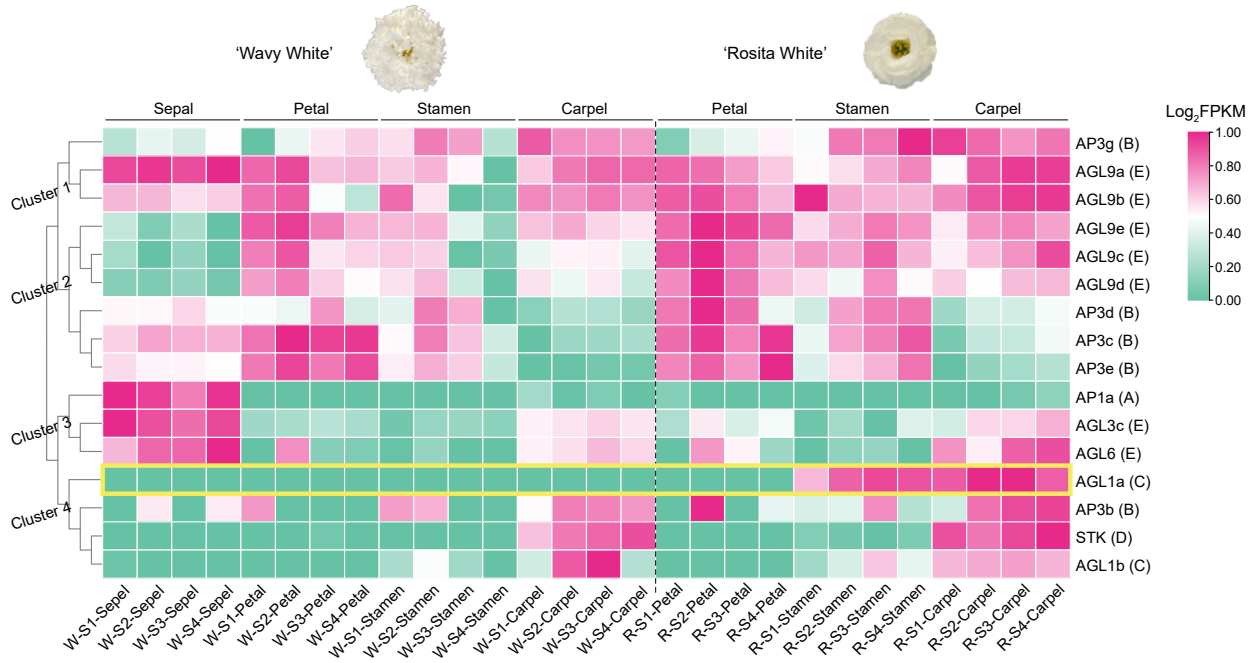

Figure S30. Heatmap of expression patterns of A-, B-, C-, D-, E-class MADS genes in 'Rosita White' (R) and 'Wavy White' (W). The MADS family genes are clustered into different categories. The MADS that might cause the difference of the double-flower phenotype (petal number) between these two varieties is framed in the yellow box. Genes with a maximum FPKM of less than 10 are not shown. The letters in brackets represent the class to which the gene belongs. The bud stage, S1; the turning stage, S2; the blooming stage, S3.

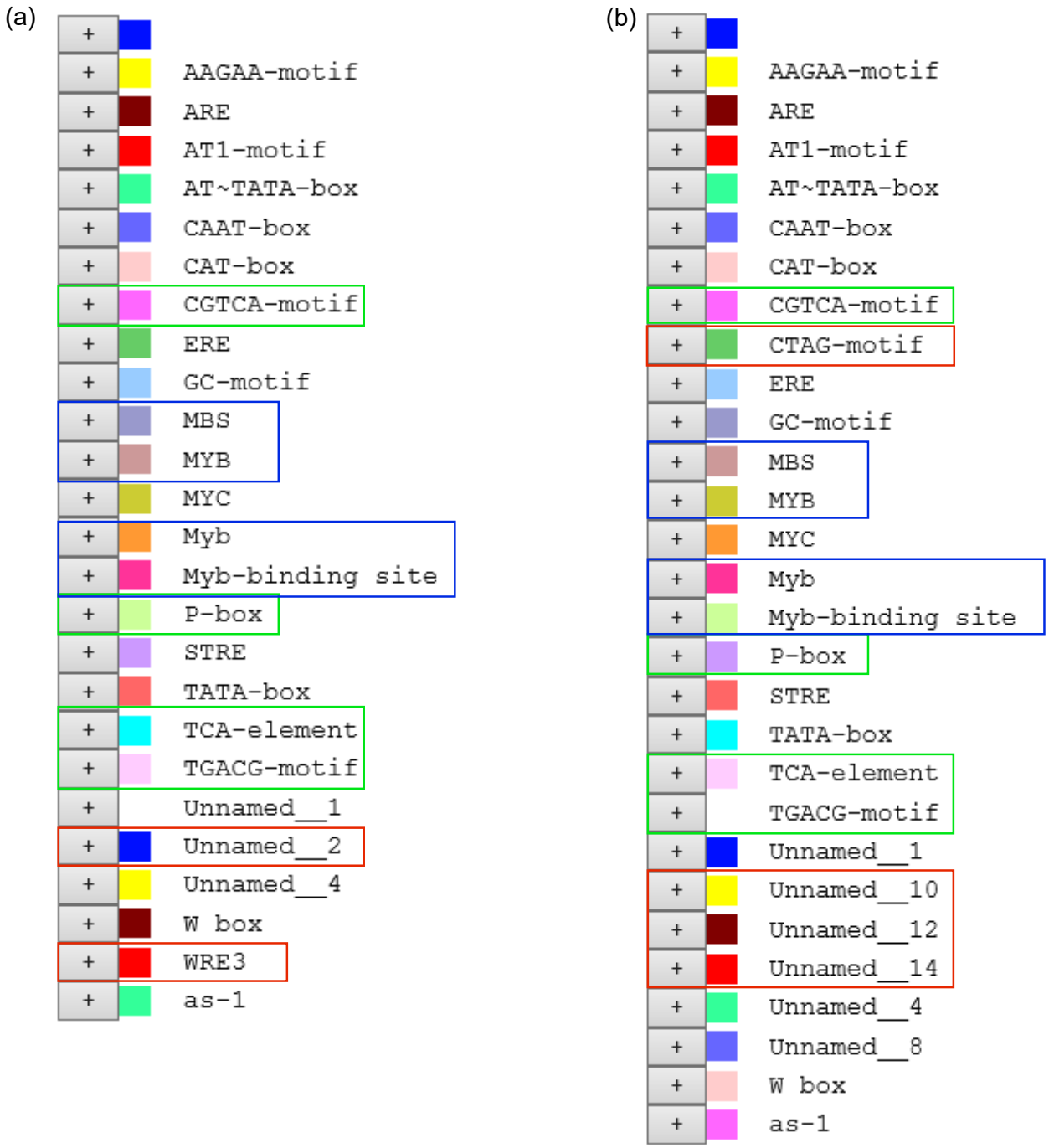

Figure S31. Analysis of cis-acting regulatory elements in the promoter of 'Wavy White' (a) and 'Rosita White' (b).

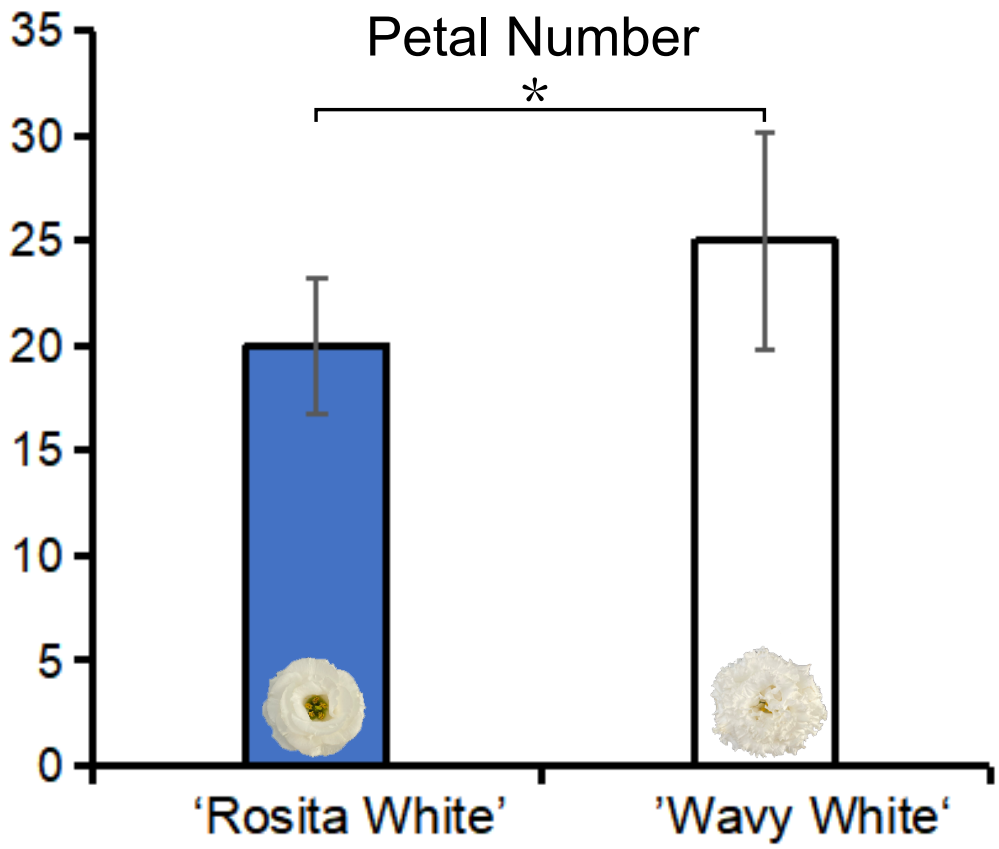

Figure S32. Statistic of petal numbers of ‘Rosita White’ and ‘Wavy White’.